Wefer, G., Berger, W.H., and Richter, C. (Eds.)
Proceedings of the Ocean Drilling Program, Scientific Results Volume 175

21. Walvis Paradox Confirmed for the Early Quaternary at the Southern End of the Namibia Upwelling System, ODP Site 1085[1]

Patricia A. Anderson,[2] Christopher D. Charles,[2] and Wolfgang H. Berger[2]

ABSTRACT

The Walvis Paradox states that opal accumulation fluctuates in counterphase to general productivity on Walvis Ridge, off northern Namibia. Sediments of early Quaternary age from Site 1085 (Cores 175-1085A-7H to 10H, off South Africa) were studied to check the phase relationships of general productivity and opal deposition in the region off the Oranje River, near the southern end of the Namibia upwelling system. The proxies used are $\delta^{18}O$ of *Cibicidoides wuellerstorfi,* $\delta^{13}C$ of *C. wuellerstorfi,* benthic foraminifers per gram (BF/g), *Uvigerina* spp. per gram (U/g), estimated diatom abundance (EDA) and sulfide and oxide aggregates (SOA) in the coarse fraction. EDA and BF/g are taken to indicate diatom and organic matter productivity, respectively. Oxygen isotopes were used to determine phase within the glacial–interglacial cycles.

The phase relationships between the different proxies emerge when applying internal stacking methods. For Core 175-1085A-7H, five prescribed 41-k.y. cycles were combined into an average 41-k.y. cycle for the different indices. Productivity indices (BF/g and U/g) tend to follow $\delta^{18}O$ in the accustomed manner (with glacial periods showing maximum productivity), but not EDA, whose maximum appears closer to interglacials, offset toward cooling. Thus, phase relationships are similar to those on Walvis Ridge, extending the Walvis Paradox to the southern end of the Namibia upwelling system for the early Quaternary. A tentative reconstruction of the phase of intensity of mixing is given, based

[1]Anderson, P.A., Charles, C.D., and Berger, W.H., 2001. Walvis Paradox confirmed for the early Quaternary at the southern end of the Namibia upwelling system, ODP Site 1085. *In* Wefer, G., Berger, W.H., and Richter, C. (Eds.), *Proc. ODP, Sci. Results,* 175, 1–31 [Online]. Available from World Wide Web: <http://www-odp.tamu.edu/publications/175_SR/VOLUME/CHAPTERS/SR175_21.PDF>. [Cited YYYY-MM-DD]
[2]Scripps Institution of Oceanography, University of California, San Diego, La Jolla CA 92093, USA. Correspondence author: **wberger@ucsd.edu**

Initial receipt: 5 July 2000
Acceptance: 14 June 2001
Web publication: 13 September 2001
Ms 175SR-201

on the two productivity indicators EDA and BF/g. Mixing is strongest during the glacial maximum.

INTRODUCTION

The coastal upwelling region off southwestern Africa associated with the Benguela Current in the eastern South Atlantic is one of the great centers of productivity in the world ocean. The goal of Ocean Drilling Program Leg 175 was to recover the materials necessary to reconstruct the Neogene history of upwelling off western Africa, south of the equator. Here we report on a study of the early Quaternary sediments recovered at Site 1085, located well off the Oranje River, south of Luederitz (Namibia) and north of Cape Town (South Africa). Site 1085 has a complex record, including evidence from coastal upwelling, from Oranje River influx, from the Benguela Current itself near the point of its origin, and from the warm water eddies spawned by the Agulhas Retroflection south of the Cape (Fig. F1). Background information on these processes may be found in a symposium on upwelling off southwestern Africa (Summerhayes et al., 1992), in a recent symposium on South Atlantic oceanography (Wefer et al., 1996), and in the Leg 175 *Initial Reports* volume (Wefer, Berger, Richter, et al., 1998), including the paleoceanographic synthesis (Berger et al., 1998). The role of upwelling in the global carbon cycle is discussed by Schneider and Müller (1995) and other authors in the same symposium (Summerhayes et al., 1995).

F1. Location of Site 1085, off southern Namibia, p. 17.

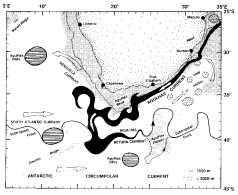

Here, we address a single question, one that arose previously from observations on Walvis Ridge, that is, the "Walvis Paradox" (Berger and Wefer, 1996). The paradox juxtaposes evidence for low opal accumulation during glacial periods in the Quaternary (Diester-Haass, 1985) with evidence for intensified upwelling and high general production during glacials (Oberhänsli, 1991). We attempt to establish whether the paradox is valid for the southernmost end of the Namibia upwelling system (and hence, presumably for the entire system from the Oranje River to the Walvis Ridge) for the early Quaternary. We shall present evidence that it is indeed valid, and we comment on the implications for variations in silicate supply and intensity of mixing for the Namibia upwelling system.

MATERIALS, METHODS, AND DATA

Source of Material

Hole 1085A is situated at the African rim of the Cape Basin at a depth of 1713.1 m on the continental slope. The position is given as 29°2.5′S, 13°9.4′E (Shipboard Scientific Party, 1998). Sediments of early Quaternary age, according to shipboard results, have accumulation rates between 35 and 100 m/m.y. We analyzed samples from Cores 175-1085A-7H through 10H. Sample spacing was 20-cm intervals; the total number of samples analyzed was 196.

Sediments of Quaternary age at Site 1085 are just over 90 m thick (average sedimentation rate near 5 cm/k.y.) and consist of greenish gray nannofossil-foraminifer ooze (Shipboard Scientific Party, 1998). Finely disseminated pyrite is common. Gas concentrations are moderate at Site 1085, and cores show much less expansion than for the immediately preceding sites occupied closer to the upwelling centers. Quater-

nary and Pliocene sediments were retrieved by hydraulic piston coring in advance of the drill bit.

General Strategy

We selected Cores 175-1085A-7H through 10H for study to investigate variations in productivity within the early Quaternary. Our samples span the period from ~1.9 to 1.1 Ma. We are only interested, in this context, in the phase of productivity-related indices relative to glacial–interglacial climatic fluctuations. Our purpose is not to provide a complete isotope stratigraphy for this interval, a task made difficult by the gaps we suspect to be present between the cores (cf. composite depth assignments in Shipboard Scientific Party, 1998). Our age assignments, consequently, are tentative. They might be helpful in work by others on these cores and are given for this reason only.

In pursuing the question of phasing of productivity, we use the fact that the early Quaternary is dominated by the 41-k.y. cycle in the global ocean $\delta^{18}O$ record (Shackleton et al., 1990; Berger and Jansen, 1994). We assume that the 41-k.y. cycle, likewise, is important at Site 1085 within the early Quaternary. Based on this assumption, we take the dominant cycle closest to 40-k.y. length within each core (as found by spectral analysis of single-core series dated by shipboard age assignments) as, in fact, representing the 41-k.y. cycle. Also, we restrict our analysis to the one core (Core 175-1085A-7H) where this cycle apparently is best represented. We present the data from the other cores, as well, to justify the selection of Core 175-1085A-7H. However, we largely ignore the data from Cores 175-1085A-8H through 10H in terms of providing evidence bearing on the question addressed. These data might prove useful in additional work on Site 1085 and in contexts not here contemplated.

Proxies were selected for (inferred) relevancy to productivity reconstruction and for ease of determination. The proxies here used are $\delta^{18}O$ of *Cibicidoides wuellerstorfi,* $\delta^{13}C$ of *C. wuellerstorfi,* benthic foraminifers per gram (BF/g), *Uvigerina* spp. per gram (U/g), visually estimated abundance (EDA) of biogenic silica (mainly diatom debris), and visually estimated abundance of iron (hydr)oxides and sulfides (SOA) and similar particles (mainly pyrite). The indices EDA and BF/g are taken to reflect diatom flux and carbon flux, respectively. BF/g is assumed to depend on the amount of carbon that settles from the productive surface waters to the seafloor. The higher the surface productivity, the more carbon reaches the seafloor, and the more benthic foraminifers can thrive (Herguera and Berger, 1991). In addition, U/g and $\delta^{13}C$ of *C. wuellerstorfi* are used to estimate relative changes in conditions regarding oxygen content and nutrient supply. To complement the data presented here, we also use the data available from shipboard analyses as published in the *Initial Reports* volume (Wefer, Berger, Richter, et al., 1998).

Sample Preparation

For this study, 196 20-g samples were obtained from Cores 175-1085A-7H, 8H, 9H, and 10H. The sampling was at 20-cm intervals, starting from the top of each core. The approximate sedimentation rate (based on shipboard data) is 4 to 5 cm/k.y. Thus, the 20-cm sampling interval typically has a resolution of between 4 and 5 k.y. For each sample, half the original amount was washed to obtain the coarse fraction containing the foraminifers, using standard laboratory techniques (de-

tails in Anderson, 2000). The average sand fraction was typically ~10% by weight. The coarse-fraction samples were then split into halves, one for reference, the other for use. The used half was further sieved into three size fractions: >250, 150–250, and 63–150 µm. A "coarse" sand fraction (>250 µm) was measured as the percent coarse sand of total sand.

Measurements and Indices

The isotopic data generated for this project were obtained for two species of benthic foraminifers: *Cibicides,* an epifaunal species, and *Uvigerina peregrina,* an infaunal species. Both $\delta^{18}O$ and $\delta^{13}C$ were measured using the Finnigan stable isotope mass spectrometer (model number MAT252) at Scripps Institution of Oceanography. The $\delta^{18}O$ index is made up of *C. wuellerstorfi* $\delta^{18}O$ measurements. Where there were no actual measurements from *C. wuellerstorfi* the measurement of *Uvigerina* – 0.92‰ was used in its place. All of the $\delta^{18}O$ Fourier analyses are based on the merged $\delta^{18}O$ series. The shift of 0.92‰ in oxygen isotopes of *Uvigerina* spp. for these early Quaternary sediments is larger than that found for more recent sediments off Peru (~0.6‰) (Dunbar and Wefer, 1984) but close to the one given by Woodruff et al. (1980) for recent benthic foraminifers of the deep-sea environment.

Data series were constructed for $\delta^{13}C$ of the two species in the same manner as for the $\delta^{18}O$. Similar to $\delta^{18}O$, an offset proved to be just as accurate as the regression equation. The difference between $\delta^{13}C$ of *C. wuellerstorfi* and $\delta^{13}C$ of *Uvigerina* is typically >1‰, which may be compared with the difference of 0.8‰ stated in Woodruff et al. (1980). No attempt was made to ascribe special significance to the $\delta^{13}C$ values of *Uvigerina* as an infaunal taxon (Zahn et al., 1986; McCorkle et al., 1990; Wefer and Berger, 1991; Mackensen and Bickert, 1999). A systematic error is likely to be present (increased organic carbon supply resulting in more negative delta values in *Uvigerina*), and results should be read with the appropriate caution.

U/gram was calculated by counting the number of specimens of *Uvigerina* in one-half of the washed split >250 µm. This number was doubled to account for the reference half. This new value was divided by the dry weight of the entire sample before washing to obtain the U/g values.

BF/g denotes benthic foraminifers per gram of total dry sample. The foraminifers were noted as a fraction of total sand, whose ratio to total sediment was determined before splitting and counting.

EDA is based on visual inspection of smear slides made from the (unwashed) reference half of the original sample. The manner of determination was suggested by Carina Lange and is described in Wefer, Berger, Richter, et al. (1998), where smear slide diatom abundances are listed for Site 1085 and other Leg 175 sites. Lange et al. (2000) have shown that smear slide estimates of diatom abundance correspond closely to measured opal content in these sediments.

SOA abundance (sulfide and oxide aggregates) was recorded in nearly all of the samples in the >250-µm size fraction as aggregates of iron sulfide and iron oxide-hydroxide, such as fillings, casts, and similar precipitates. Both SOA and EDA indices are subjective estimates of ranked abundance (from "barren" to "extremely abundant" [0 to 6]) based on microscope observations. No chemical analyses were performed on the materials.

Percent sand is the dry weight of the residue after washing on a 63-µm sieve as a ratio to the total dry weight of the sample before washing. Percent coarse sand is the percentage of the sand fraction >250 µm. Within calcareous ooze, sand content may be taken as a clue to preservation of foraminifer shells, that is, as a dissolution index (Johnson et al., 1977).

Depth and Age Assignments

Depth and age assignments are listed in the "Appendix," p. 15, where the method leading from driller's depth to final depth is described. We used spectral analysis to estimate the in situ sedimentation rate based on the assumption that 41-k.y. cycles are present in these early Quaternary sediments. Our age assignments do not differ substantially from interpolations of shipboard tie points. In fact, they are not crucial to the arguments regarding the Walvis Paradox. These arguments deal with the phase of various proxy parameters within a typical obliquity cycle whose precise position within the early Quaternary is immaterial. We offer the depth and age assignments here because they might prove useful in other contexts.

The sedimentation rates arrived at by the procedure outlined in the "Appendix," p. 15, range from 3.61 cm/k.y. for Core 175-1085A-7H to 9.81 cm/k.y. for Core 10H (see Fig. F2). They decrease upward, most rapidly in the early portion of the interval studied, presumably as a result of changes in sediment supply by the Oranje River or from an increase in bottom current activity, or both.

Core 175-1085A-7H has a strong, well-defined 41-k.y. signal showing a dominant obliquity cycle in the oxygen isotope record. Only minor adjustment was necessary to bring the peak into focus (Table T1). The other cores (Cores 175-1085A-8H, 9H, and 10H) have spectra that are less clearly tied to obliquity (or other Milankovitch forcing). Core 175-1085A-7H, having the strongest signal, is used as a template for examining the phase between proxies.

RESULTS: CLIMATE- AND PRODUCTIVITY-RELATED PROXIES

Stable Isotopes

The record of oxygen isotope ratios that emerges after age assignment as described may be taken as depicting climate state (Fig. F3). Well-expressed cycles are seen in Core 175-1085A-7H. In the older sediments, cyclicity is less well expressed and overall the amplitudes tend to be lower as well. The record of Core 175-1085A-8H has substantial gaps owing to the scarcity of *C. wuellerstorfi* in certain intervals. (In what follows, this is remedied by merging with adjusted *Uvigerina*. We have not assigned isotope stages to these data, as the precise stratigraphic position of the records within the cores is in some doubt and is immaterial to the argument of this paper.)

The record of the carbon isotope ratios reflects both deep-ocean ventilation and the regional addition of carbon dioxide from the combustion of organic matter on the way to and on the seafloor. The carbon isotope series is seen to be shifted by somewhat different amounts, with respect to oxygen isotopes, in the three cores for which data are available (Fig. F4). The shift consists in a slight lag of $\delta^{13}C$, from which one

F2. Sedimentation rates obtained from depth adjustments and age assignments, p. 18.

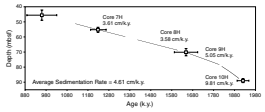

T1. Sedimentation rate adjustments based on Fourier analysis of oxygen isotope records, p. 26.

F3. Stable isotope record of Cores 175-1085A-7H, 8H, 9H, and 10H, p. 19.

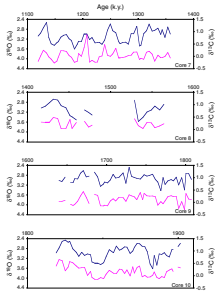

F4. Correlation between oxygen isotope and carbon isotope series, p. 20.

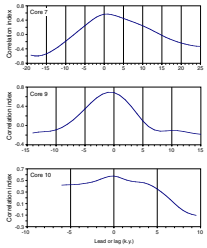

might tentatively conclude that the carbon cycle (and deep ventilation) follows rather than leads climate change. However, the relationship of the carbon isotope record at any one location to the global change in carbon cycling (and atmospheric carbon dioxide) is not readily ascertained.

As described in **"Materials, Methods, and Data,"** p. 2, the cycle closest to a 40-k.y. period was used for age assignment. Among the four cores studied, Core 175-1085A-7H has the most prominent 41-k.y. cycle, as readily seen in the Fourier spectra (Fig. **F5**). The record of Core 175-1085A-7H also has the only cycle that might qualify as a ~100-k.y. eccentricity cycle, as well as a possible 23-k.y. cycle. No claim is made (or seems advisable) regarding the presence or prominence of cycles in the other cores, given this limited analysis. Neither is this necessary given the purpose of the study.

BF/g as a Productivity Index

The index BF/g is a stand-in for the accumulation rate of benthic foraminifers, which in turn is closely related to the supply of organic matter to the seafloor, and therefore, to export production (Altenbach and Sarnthein, 1989; Herguera and Berger, 1991; Loubere, 1994; Fariduddin and Loubere, 1997). We do not use benthic foraminifer accumulation rate (BFAR) because we have not determined changes of sedimentation rate within the 41-k.y. cycles. We assume that BF/g reflects accumulation rate sufficiently well to show the glacial–interglacial contrast in productivity, if any. In principle, the higher the surface productivity, the more carbon reaches the seafloor, and the more benthic foraminifers can thrive (Herguera and Berger, 1991).

In Core 175-1085A-7H, the abundance of benthic foraminifers expressed on a logarithmic scale is perfectly in phase with the oxygen isotope curve, such that warm intervals show low abundance and cold intervals high abundance (Fig. **F6A**). The regression coefficient is near 0.4 and is highly significant. In the other cores, the same overall relationship is observed but the details are more complicated (Fig. **F6B, F6C, F6D**). In particular, there is a tendency for peak highs and lows to occur not in line with climate extremes (as seen in the oxygen isotopes) but offset by between 5 and 10 k.y.

EDA as a Productivity Index

EDA, being closely related to diatom abundance, should provide an excellent index for productivity. Estimated diatom abundance on the present-day seafloor is clearly tied to upwelling regions (e.g., Barron and Baldauf, 1989; Baldauf and Barron, 1990; Charles et al., 1991; Berger and Herguera, 1992). We first check the relationship of EDA to the glacial–interglacial cycle as seen in Core 175-1085A-7H (which shows the strongest cycles). To simplify the task of finding phase relationships, we only consider cycles in the 41-k.y. band, which we generate by inverting the portion in the Fourier matrix that surrounds the 41-k.y. cycle (Fig. **F7A**). After such filtering, different indices are readily compared. Results of the Fourier analysis show a negative correlation between $\delta^{18}O$ and EDA, at least for the upper half of Core 175-1085A-7H in the central part of the Pleistocene (see Fig. **F7B**). This result is reminiscent of the situation reported for the Walvis Ridge (Deep Sea Drilling Project Site 532) (Hay et al., 1984; Diester-Haass 1985). The reasons for the negative correlation are not clear. Taking the data at face

F5. Fourier spectrum of the $\delta^{18}O$ stratigraphy of the cores studied, p. 21.

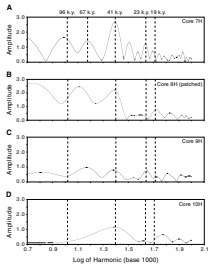

F6. Benthic foraminifer abundance compared with climatic state, p. 22.

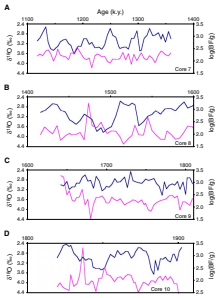

F7. Comparison of $\delta^{18}O$ and EDA within the 41-k.y. cycle, p. 23.

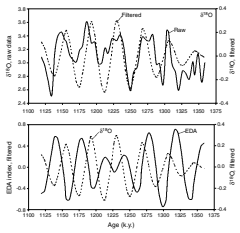

value, either productivity is lower during glacial times than during interglacials (contrary to expectations and to the results from the abundance of benthic foraminifers) or the index EDA does not reflect overall productivity (see "Discussion: Walvis Paradox and Phase Relationships," p. 8).

Uvigerina $\delta^{13}C$ Record

The $\delta^{13}C$ record of benthic foraminifers is related to oxygen consumption and nutrient content in deep waters (Berger and Vincent, 1986; Zahn et al., 1986; McCorkle et al., 1990), export production (Mackensen and Bickert, 1999), and exchange processes between ocean and atmosphere (Charles et al., 1993). To make some simple comparisons regarding glacial–interglacial contrast, we selected 11 samples from Cores 175-1085A-7H and 10H for detailed analysis; six of these have high $\delta^{18}O$ values for *C. wuellerstorfi,* and five have low values (10 percentile). The samples were analyzed for the corresponding isotope values for *Uvigerina peregrina,* and these values were use to define the environmental space.

Typical interglacial values for $\delta^{13}C$ of *Uvigerina* (low $\delta^{18}O$ in *C. wuellerstorfi*) scatter around –0.9‰, and glacial values around –1.15‰, for a difference of 0.25‰. This is slightly more than one-half the glacial–interglacial contrast in deep water for the late Quaternary in this setting (Mackensen and Bickert, 1999) but much less than the overall range expected (Raymo et al., 1997). The change in deep water composition is a general background signal presumably related to glacial input of terrigenous organic carbon (Shackleton, 1977) and to changes in deep ocean oxygen utilization and ventilation (Boyle, 1988; Raymo et al., 1997). From the diminished glacial–interglacial contrast observed, it can be surmised that the oxygen utilization within the water bathing the seafloor at Site 1085 was decreased during maximum glaciation in the early Quaternary.

To test whether EDA is more closely related to *Uvigerina* $\delta^{13}C$ than to *Uvigerina* $\delta^{18}O$, with which it is negatively correlated (Fig. F7), we chose 12 samples, 6 with high and 6 with low values of EDA, and which also have isotopic values for *Uvigerina.* High EDA tends to occur with low $\delta^{18}O$ of *Uvigerina* and high $\delta^{13}C$ of Uvigerina, indicating that diatom production is high during interglacial conditions.

SOA Patterns

Twelve samples, six with high and six with low values (10 percentile), were selected for investigation of SOA patterns. Only samples containing *Uvigerina* were chosen, and the *Uvigerina* specimens picked were analyzed for stable isotopes. High SOA values (mainly pyrite) go with interglacial conditions and vice versa. Surprisingly, there is more coarse pyrite in the interglacial.

Why should there be more SOA associated with the interglacial periods? Several reasons are possible. There may actually be more pyrite in the glacial sections, but it may be more finely disseminated and not emerge in the coarse fraction. Or it may be diluted by increased terrigenous input. Delivery of iron may change greatly on a glacial–interglacial timescale, with chemical weathering (and supply of SOA) less important during glacial periods. Finally, conditions of diagenesis may change markedly from glacial to interglacial conditions. When produc-

tivity is high, iron (hydr)oxides are quickly reduced and made mobile, and reduction of sulfate provides sulfide to trap iron and related SOAs. With so many factors potentially playing a role, SOA cannot be expected to be a good productivity indicator. In any case, according to these results, coarse SOA parallels EDA, that is, it is anticorrelated with oxygen isotopes, being high in interglacial periods and low in glacial intervals.

DISCUSSION: WALVIS PARADOX AND PHASE RELATIONSHIPS

Modular Plots

Modular plots allow a simple visualization of phase relationships for selected climatic cycles, such as the 41-k.y. cycle extracted by Fourier analysis. By isolating the 41-k.y. cycle hidden within the original data, phase relationships can be explored, as illustrated above (Fig. **F7B**). Modular plots differ from a simple cycle extraction in that the individual cycles are combined to get an average cycle for a given interval, such as an entire core. All the cycles within such an interval are stacked and averaged; thus, a modular plot represents an internal stack of a selected cycle or period. (For a description of the method, see Berger et al., 1993.)

Modular plots comparing the various proxies with $\delta^{18}O$ *C. wuellerstorfi* were created for the following elements: sand, coarse sand, EDA, BF/g, U/g, and $\delta^{13}C$ of *C. wuellerstorfi*. Modular plots were generated for Core 175-1085A-7H, where signals were strong within the bandwidth surrounding 41 k.y. and where there are five cycles to stack. Because of the amplitude of the dominant cycle and the number of cycles, Core 175-1085A-7H is presumed to show relationships most clearly for all of the indices. Core 175-1085A-8H modular plots (not shown) were created from patched isotope data using only three 41-k.y. cycles and are much less trustworthy. Cores 175-1085A-9H and 10H have very weak 41-k.y. signals (six times weaker than those of Core 7H). Therefore, only Core 175-1085A-7H is considered as yielding reliable patterns worth discussing (Fig. **F8**).

On the whole, in Core 175-1085A-7H, the *state* of climate is more important than the *change* in conditions (Fig. **F8**). The proxies, in essence, follow $\delta^{18}O$ *C. wuellerstorfi* isotopic cycles, with the exception of EDA. The carbon isotope signal is seen to be slightly offset, showing a lag with respect to the oxygen isotope record. (The discrepancy of this result with the zero lag shown in Fig. **F4A** suggests differences in asymmetries with respect to sine-shaped cycles between the $\delta^{18}O$ and $\delta^{13}C$ 41-k.y. cycles.)

EDA abundance in Core 175-1085A-7H was quite low, as were (estimated) amplitudes in the fluctuations in abundance. Thus, whereas EDA has a reverse relationship to $\delta^{18}O$ compared with expectations if diatom supply goes parallel to productivity, it is equally valid to say that EDA simply does not change very much, no matter what the state. The low amplitude of variation does not preclude the determination of phase, however. This situation is quite similar to the one reported off Angola for the late Quaternary (Schneider, 1991; Berger et al., 1994).

F8. Modular plots for Core 175-1085A-7H, p. 24.

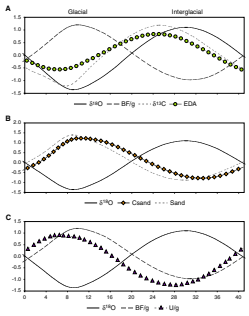

EDA Paradox and Upwelling

The modular plot analysis shows that EDA is almost as much correlated to change as to state of climate, unlike the other variables. In particular, the phases of BF/g and U/g suggest that organic matter supply is at maximum during fully glacial conditions (Fig. F8A, F8C), whereas EDA peaked more than 90° earlier and is on its way down toward a minimum at the very end of the glacial. Maximum productivity during glacial conditions, as seen in the benthic foraminifers, is also in agreement with other evidence in this region, even on Walvis Ridge (Oberhänsli, 1991). On Walvis Ridge, as mentioned, diatoms and radiolarians are likewise more abundant during interglacials (Diester-Haass et al., 1992), than during periods of high productivity.

The paradox represented by the contrary phase of silica has been discussed by a number of authors (Diester-Haass et al., 1992; Hay and Brock 1992; Berger and Wefer 1996; Berger et al., 1998). We must consider the possibility that the silicate content of the upper thermocline, from which silica for diatom frustules is derived during upwelling, changes through the glacial–interglacial cycles. This has been demonstrated for the North Pacific (Berger et al., 1997). When comparing the phosphate and silicate contents of subsurface waters, one finds that phosphate content is highly correlated with Si/P, that is, silicate is reduced more rapidly than phosphate when nutrients are extracted and it is released back more slowly to the water from sinking particles within the upper water layers (Berger and Lange, 1998). It is possible therefore, in principle, to increase productivity through upwelling in a given area without increasing diatom production. To do this, phosphate has to be brought to the site within thermocline water with a low Si/P ratio, that is, waters with low nutrient content. To overcome the handicap in quality, the upwelling and mixing has to be that much more vigorous, that is, the wind stress has to be increased greatly if productivity is to remain high despite the supply of "poor" water (Berger and Lange, 1998).

Whenever intensity of mixing of surface waters and nutrient content of subsurface waters are anticorrelated, diatom production will go through an optimum that is phase-shifted from the maximum of upwelling toward the maximum of nutrient concentration. Using this conceptual approach, we can attempt to reconstruct the (presumed) driver of mixing and upwelling, that is, "wind stress," at least qualitatively. For this purpose, we use BF/g as a proxy for productivity and we take EDA/(BF/g) as a proxy for Si/P in the water and, hence, of the quality of the upwelled water.

We then write the following:

$$\text{Productivity} = (\text{wind-driven upwelling rate}) \times (\text{nutrient concentration in upwelled water}).$$

By proxy,

$$\text{BF/g} = \text{wind} \times \text{EDA}/(\text{BF/g}),$$

so that

$$\text{wind} = (\text{BF/g})^2/\text{EDA}.$$

This qualitative reconstruction is illustrated in Figure F9.

F9. Relative strength of upwelling and mixing wind, p. 25.

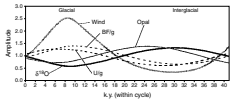

The rate of mixing and upwelling (wind) is seen to be at maximum late during glacial time, with productivity peaking early in glacial time, when nutrients have not yet reached their low point. Thus, regarding productivity, it seems that early glaciation is a privileged time, when both nutrient supply (decreasing) and wind (increasing) combine for an optimum period of productivity. Also, the modular plot (Fig. F9) suggests that intensity of mixing, in essence, has to override the effects of the low glacial nutrient supply. Apparently, it is able to do so more efficiently for phosphate and nitrate (which stimulates organic matter supply) than for silicate (which stimulates diatom growth). Presumably, this is due to nutrient stratification in the thermocline, with silicate peaking at greater depth than either phosphate or nitrate (Berger and Lange, 1998).

It would be very interesting to test the hypothesis of decreased nutrient supply in upwelling waters during glacial conditions. However, the available data appear insufficient to do this. In particular, the $\delta^{13}C$ values available for *C. wuellerstorfi* and *Uvigerina* pertain to conditions at the seafloor at 1700-m depth. In any case, our results support the concept of nutrient depletion in the glacial thermocline (Berger and Lange, 1998), whether through increased vertical fractionation (Boyle, 1988) or through increased lockup in more focused upwelling regions (Berger et al., 1994), or both.

SUMMARY AND CONCLUSIONS

A sequence within the early to middle Quaternary productivity record off southwest Africa (Core 175-1085A-7H) is strongly influenced by climate cycles at periods of 41 k.y. (obliquity driven) and also 100, 70, 23, and 19 k.y. Earlier sequences (Cores 175-1085A-9H and 10H) show less distinct periodicity. Modular analysis of various productivity-related proxies at the obliquity period within Core 175-1085A-7H shows that the proxies BF/g and EDA are not in phase. Organic matter production, as recorded in BF/g, closely follows the climate state, with maxima during glacial times. But diatom production, as seen in EDA, does not follow this pattern. Instead, it shows a low level of response to climate fluctuations, with equal influence from the climate state (as seen in $\delta^{18}O$) and its derivative (change in $\delta^{18}O$). The reason is, presumably, the depletion of thermocline waters with silicate, as also seen elsewhere in the glacial ocean, notably the North Pacific (Berger and Lange, 1998).

In the present ocean, the Si/P ratio of subsurface waters may be taken as a measure of thermocline fertility, that is, nutrient concentration in subsurface waters (Berger and Lange, 1998). From this relationship we can derive an estimate for (relative) nutrient abundance, setting Si/P = EDA/(BF/g). Once variation in nutrient abundance is captured, we can derive an estimate of relative strength of upwelling (wind) as the ratio between productivity and nutrient content of upwelled waters (Berger et al., 1994; Herguera and Berger, 1994). In the present case, the "wind" is proxied by $(BF/g)^2/EDA$. From this formulation, "wind" maxima emerge during maximum glaciation, and vice versa. This is not surprising, since the intensity of winds owes much to planetary temperature gradients, which may be taken as especially strong during glacials (Arrhenius, 1952; Flohn, 1985; Leinen and Sarnthein, 1989; Berger and Herguera, 1992).

ACKNOWLEDGMENTS

We thank Helge Arz and Lydia Dupont (both at GEO Bremen) for their careful and helpful reviews of the draft version of this paper. The work was supported by a grant from USSAC, administered by Texas A&M as part of the Ocean Drilling Program.

This research used samples and/or data provided by the Ocean Drilling Program (ODP). ODP is sponsored by the U.S. National Science Foundation (NSF) and participating countries under the management of Joint Oceanographic Institutions (JOI), Inc.

REFERENCES

Altenbach, A.V., and Sarnthein, M., 1989. Productivity record in benthic foraminifers. *In* Berger, W.H., Smetacek, V.S., and Wefer G. (Eds.), *Productivity of the Oceans: Present and Past:* New York (Springer-Verlag), 255–269.

Anderson, P.A., 2000. Early Quaternary history of productivity off South West Africa, ODP Site 1085 Hole A Leg 175 [M.S. thesis]. Univ. Calif., San Diego.

Arrhenius, G., 1952. Sediment cores from the East Pacific. *In* Pettersson, H. (Ed.), *Rep. Swed. Deep-Sea Exped., 1947–1948,* 5:189–201.

Baldauf, J.G., and Barron, J.A., 1990. Evolution of biosiliceous sedimentation patterns—Eocene through Quaternary: paleoceanographic response to polar cooling. *In* Bleil, U., and Thiede, J. (Eds.), *Geological History of the Polar Oceans: Arctic Versus Antarctic:* Dordrecht (Kluwer Academic), 575–607.

Barron, J.A., and Baldauf, J.G., 1989. Tertiary cooling steps and paleoproductivity as reflected by diatoms and biosiliceous sediments. *In* Berger, W.H., Smetacek, V.S., and Wefer, G. (Eds.), *Productivity of the Oceans: Present and Past:* New York (Wiley-Interscience), 341–354.

Berger, W.H., Bickert, T., Schmidt, H., and Wefer, G., 1993. Quaternary oxygen isotope record of pelagic foraminifers: Site 806, Ontong Java Plateau. *In* Berger, W.H., Kroenke, L.W., Mayer, L.A., et al., *Proc. ODP, Sci. Results,* 130: College Station, TX (Ocean Drilling Program), 381–395.

Berger, W.H., and Herguera, J.C., 1992. Reading the sedimentary record of the ocean's productivity. *In* Falkowski, P.G., and Woodhead, A.D. (Eds.), *Primary Productivity and Biogeochemical Cycles in the Sea:* New York (Plenum), 455–486.

Berger, W.H., Herguera, J.C., Lange, C.B., and Schneider, R., 1994. Paleoproductivity: flux proxies versus nutrient proxies and other problems concerning the Quaternary productivity record. *In* Zahn, R., Kaminski, M., Labeyrie, L.D., and Pederson, T.F. (Eds.), *Carbon Cycling of the Glacial Ocean: Constraints on the Ocean's Role in Global Change: Quantitative Approaches in Paleoceanography:* Berlin (Springer-Verlag), NATO ASI Ser., 17:385–412.

Berger, W.H., and Jansen, E., 1994. Mid-Pleistocene climate shift: the Nansen connection. *In* Johannessen, O.M., Muensch, R.D., and Overland, J.E. (Eds.), *The Role of the Polar Oceans in Shaping the Global Environment.* Geophys. Monogr., Am. Geophys. Union, 85:295–311.

Berger, W.H., and Lange, C.B., 1998. Silica depletion in the thermocline of the glacial North Pacific: corollaries and implications. *Deep-Sea Res.,* 45:1885–1904.

Berger, W.H., and Vincent, E., 1986. Deep-sea carbonates: reading the carbon-isotope signal. *Geol. Rundsch.,* 75:249–269.

Berger, W.H., Lange, C.B., and Weinheimer, A., 1997. Silica depletion of the thermocline in the eastern North Pacific during glacial conditions: clues from Ocean Drilling Program Site 893, Santa Barbara Basin, California. *Geology,* 25:619–622.

Berger, W.H., and Wefer, G., 1996. Expeditions into the past: paleoceanographic studies in the South Atlantic. *In* Wefer, G., Berger, W.H., Siedler, G., Webb, D.J. (Eds.), *The South Atlantic: Present and Past Circulation:* Berlin (Springer-Verlag), 363–410.

Berger, W.H., Wefer, G., Richter, C., Lange, C.B., Giraudeau, J., Hermelin, O., and Shipboard Scientific Party, 1998. The Angola-Benguela upwelling system: paleoceanographic synthesis of shipboard results from Leg 175. *In* Wefer, G., Berger, W.H., and Richter, C., et al., *Proc. ODP, Init. Repts.,* 175: College Station, TX (Ocean Drilling Program), 505–531.

Boyle, E.A., 1988. The role of vertical chemical fractionation in controlling late Quaternary atmospheric carbon dioxide. *J. Geophys. Res.,* 93:15701–15714.

Charles, C.D, Froelich, P.N., Zibello, M.A., Mortlock, R.A., and Morley, J.J., 1991. Biogenic opal in southern ocean sediments over the last 450,000 years: implications for surface water chemistry and circulation. *Paleoceanography,* 6:697–728.

Charles, C.D., Wright, J.D., and Fairbanks, R.G., 1993. Thermodynamic influences on the marine carbon isotope record. *Paleoceanography,* 8:691–697.

Diester-Haass, L., 1985. Late Quaternary upwelling history off southwest Africa (DSDP Leg 75, HPC 532). *In* Hsü, K.J., and Weissert, H.J. (Eds.), *South Atlantic Paleoceanography:* Cambridge (Cambridge Univ. Press), 47–55.

Diester-Haass, L., Meyers, P.A., and Rothe, P., 1992. The Benguela Current and associated upwelling on the southwest African margin: a synthesis of the Neogene-Quaternary sedimentary record at DSDP Sites 362 and 352. *In* Summerhayes, C.P., Prell, W.L., and Emeis, K.C. (Eds.), *Upwelling Systems: Evolution Since the Early Miocene*. Spec. Publ.—Geol. Soc. London, 64:331–342.

Dunbar, R.B., and G. Wefer, 1984. Stable isotope fractionation in benthic foraminifera from the Peruvian continental region. *Mar. Geol.,* 59:215–225.

Fariduddin, M., and Loubere, P., 1997. The surface ocean productivity response of deeper water benthic foraminifera in the Atlantic Ocean. *Mar. Micropaleontol.,* 32:289–310.

Flohn, H., 1985. Das Problem der Klimaänderungen in Vergangenheit und Zukunft. *Wiss. Buchgesellschaft,* Darmstadt.

Hay, W.W., and Brock, J.C., 1992. Temporal variation in intensity of upwelling off southwest Africa. *In* Summerhayes, C.P., Prell, W.L., and Emeis, K.C. (Eds.), *Upwelling Systems: Evolution Since the Early Miocene.* Spec. Publ.—Geol. Soc. London, 64:463–497.

Hay, W.W., Sibuet, J.C., et al., 1984. Site 532: Walvis Ridge. *Init. Repts. DSDP,* 75: Washington (U.S. Gov. Printing Office), 295–445.

Herguera, J.C., and Berger, W.H., 1991. Paleoproductivity: glacial to postglacial change in the western equatorial Pacific, from benthic foraminifera. *Geology,* 19:1173–1176.

————, 1994. Glacial to postglacial drop of productivity in the western equatorial Pacific: mixing rate versus nutrient concentrations. *Geology,* 22:629–632.

Johnson, T.C., Hamilton, E.L., and Berger, W.H., 1977. Physical properties of calcareous ooze: control by dissolution at depth. *Mar. Geol.,* 24:259–277.

Lange, C.B, Berger, W.H., Lin, H.-L., Wefer, G., and Shipboard Scientific Party, 1999. The early Matuyama diatom maximum off SW Africa, Benguela Current System (ODP Leg 175). *Mar. Geol.,* 161:93–114.

Leinen, M., and Sarnthein, M., 1989. *Paleoclimatology and Paleometeorology: Modern and Past Patterns of Global Atmospheric Transport:* Doldrecht (Kluwer).

Loubere, P., 1994. Quantitative estimation of surface ocean productivity and bottom water oxygen concentration using benthic foraminifers. *Paleoceanography,* 9:723–737.

Lutjeharms, J.R.E., and van Ballegooyen, R.C., 1988. The retroflection of the Agulhas Current. *J. Phys. Oceanog.,* 18:1570–1583.

Mackensen, A., and T. Bickert, 1999. Stable carbon isotopes in benthic foraminifera: proxies for deep and bottom water circulation and new production. *In* Fischer, G., and Wefer, G., (Eds.) *Use of Proxies in Paleoceanography.* Berlin Heidelberg (Springer Verlag): 229–254.

McCorkle, D.C., Keigwin, L.D., Corliss, B.H., and Emerson, S.R., 1990. The influence of microhabitats on the carbon isotopic composition of deep sea benthic foraminifera. *Paleoceanography,* 5:161–185.

Oberhänsli, H., 1991. Upwelling signals at the northeastern Walvis Ridge during the past 500,000 years. *Paleoceanography,* 6:53–71.

Peterson, R.G., and Stramma, L., 1991. Upper-level circulation in the South Atlantic Ocean. *Progr. Oceanogr.,* 26:1–73.

Raymo, M.E., Oppo, D.W., and Curry, W., 1997. The mid-Pleistocene climate transition: a deep sea carbon isotopic perspective. *Paleoceanography,* 12:546–559.

Schneider, R., 1991. Spätquartäre Produktivitätsänderungen im östlichen Angola-Becken: Reaktion auf Variationen im Passat-Monsun-Windsystem und in der

Advektion des Benguela-Küstenstroms [Ph.D. thesis]. *Ber. Fachber. Geowiss.,* 21. Univ. Bremen, Germany.

Schneider, R.R., and Müller, P.J., 1995. What role has upwelling played in the global carbon and climate cycles on a million-year time scale? *In* Summerhayes, C.P., Emeis, K.-C., Angel, M.V., Smith, R.L., and Zeitzschel, B. (Eds.) *Upwelling in the Ocean: Modern Processes and Ancient Records,* London (John Wiley & Sons), 361–380.

Shackleton, N.J., 1977. Carbon-13 in *Uvigerina:* tropical rainforest history and the equatorial Pacific carbonate dissolution cycles. *In* Andersen, N.R., and Malahoff, A. (Eds.), *The Fate of Fossil Fuel CO_2 in the Oceans:* New York (Plenum), 401–427.

Shackleton, N.J., Berger, A., and Peltier, W.A., 1990. An alternative astronomical calibration of the lower Pleistocene timescale based on ODP Site 677. *Trans. R. Soc. Edinburgh: Earth Sci.,* 81:251–261.

Shipboard Scientific Party, 1998. Site 1085. *In* Wefer, G., Berger, W.H., and Richter, C., et al., *Proc. ODP, Init. Repts.,* 175: College Station, TX (Ocean Drilling Program), 385–428.

Summerhayes, C.P., Emeis, K.C., Angel, M.V., Smith, R.L., and Zeitschel, B., 1995. *Upwelling in the Ocean: Modern Processes and Ancient Records:* New York (Wiley and Sons), Dahlem Workshop Reports.

Summerhayes, C.P., Prell, W.L., Emeis, K.C. (Eds.), 1992. Upwelling Systems: Evolution Since the Early Miocene. *Spec. Publ.—Geol. Soc. London,* 64.

Wefer, G., and Berger, W.H., 1991. Isotope paleontology: growth and composition of extant calcareous species. *Mar. Geol.,* 100:207–248.

Wefer, G., Berger, W.H., Siedler, G., and Webb, D.J. (Eds.), 1996. *The South Atlantic: Present and Past Circulation:* Berlin (Springer-Verlag).

Wefer, G., Berger, W.H., Richter, C., and Shipboard Scientific Party, 1998. Facies patterns and authigenic minerals of upwelling deposits off southwest Africa. *In* Wefer, G., Berger, W.H., and Richter, C., et al., *Proc. ODP, Sci. Results,* 175: College Station, TX (Ocean Drilling Program), 487–504.

Woodruff, F., Savin, S.M., and Douglas, R.G., 1980. Biological fractionation of oxygen and carbon isotopes by Recent benthic foraminifera. *Mar. Micropaleontol.,* 5:3–11.

Zahn, R., Winn, K., and Sarnthein, M., 1986. Benthic foraminiferal $\delta^{13}C$ and accumulation rates of organic carbon: *Uvigerina peregrina* group and *Cibicidoides wuellerstorfi*. *Paleoceanography,* 1:27–42.

APPENDIX

Data for Hole 1085A

Table AT1 gives the data for Hole 1085A, located at 29°22.5′S, 13°59.4′E (water depth = 1713 m, penetration = 604 meters below seafloor [mbsf]).

AT1. Data for Hole 1085A, p. 27.

The sample number column shows lab numbers assigned in the order of arrival from the Ocean Drilling Program Bremen repository. The rows are in ascending order of core and section number, starting with Core 175-1085A-7H. The depth entries are as given on the labels on the packaging in which the samples arrived. Revised depth, final depth, initial age, and final age estimate were obtained as described below. The remainder of the column entries contain the various data collected (see text). If no data were collected, it was either because the sample was not chosen for analysis or because the sample was unsuitable (e.g., absence of the species to be analyzed, in the case of *C. wuellerstorfi)*. The comments column contains numbered comments referring to sample content such as clumps, fish tooth, and so on, as listed in the table notes.

The path from driller's depth to final depth has an intermediate step labeled revised depth. To fine-tune the age estimates for the samples, we first need to fine-tune the depths and reconcile the shipboard ages with the new depths. In the last step, we use spectral analysis to estimate the in situ sedimentation rate based on the assumption that 41-k.y. cycles are present in these early Quaternary sediments. We used the composite depth assignments made on board ship for a first estimate of expansion and gap size between cores.

The revised depth was calculated to compensate for core expansion. In estimating the effect on apparent depth in core, we keep the driller's depth for the top of each core. We assume core expansion of 10% and calculate new depths on this basis. This eliminates the problem of overlapping core depths due to expansion. A 10% expansion is chosen based on typical offset values when splicing the magnetic record of Hole 1085A with that of Hole 1085B (see Shipboard Scientific Party, 1998, table 8). (For comparison, in Leg 130 cores, which contain much less organic carbon, typical expansion values were near 6%; Berger et al., 1993). A 10% expansion also takes account of the fact that there are gaps between successive cores.

The final depth is based on the driller's depth for the top of Core 175-1085A-7H, the correction for expansion, and an adjustment for the gaps between Cores 7H to 10H to account for loss of sediment and the portions of core ends that were not sampled. This was done by using core recovery data and by estimating and connecting the (presumed) 41-k.y. cycles between cores. Core 175-1085A-8H apparently had substantial loss of well over a meter, most likely from the top of the section. We have assigned new depths to core top to account for the inferred loss: Core 175-1085A-8H top depth was reset downward by 1.22 m. Also, Core 175-1085A-9H top depth was reset upward by 0.35 m, and Core 10H top depth was reset downward by 0.84 m.

Leg 175 shipboard stratigraphic data are used for preliminary age assignments. Ages are calculated in a four-step process, initial age, revised age, approximate age, and final age estimate. The initial age is based on a simple interpolation between the biostratigraphic events listed in table 2 of the Site 1085 report (Shipboard Scientific Party, 1998). Revised age reconciles the initial age to the adjusted depths assigned to samples to compensate for core expansion and partial recovery. Approximate

age is an adjustment of ages employing the final depth and position of the (assumed) 41-k.y. cycle extracted from $\delta^{18}O$ stratigraphy. Using spectral analysis based on this approximate age, a final age estimate is generated in sharpening the peaks for the 41-k.y. cycle (see Table **T1**).

Four fix-point ages were used for initial age as follows. Each sample was given an initial age based on connecting tie points, by a smooth-fit curve. The estimated depth is the mean between the upper and lower depth of constraint for the event reported; the suggested uncertainty is near 2 m. The fix-point ages are as follows:

1. Tie point = 0.96 Ma; initial depth = 45.57 mbsf.
2. Tie point = 1.25 Ma; initial depth = 55.65 mbsf.
3. Tie point = 1.67 Ma; initial depth = 70.74 mbsf.
4. Tie point = 1.95 Ma; initial depth = 90.99 mbsf.

The tie points are in excellent agreement with paleomagnetic data (Shipboard Scientific Party, 1998; table 7).

To obtain the revised age, initial depths were replaced by revised depths, keeping the initial age for the samples closest to each tie point and recalculating the sedimentation rate. After determining final depths for each sample, the reapplication of this same procedure yields approximate age. The final age estimate is calculated by running a spectral analysis on the $\delta^{18}O$ data, tagged by approximate ages. From the extraction of the (presumed) 41-k.y. cycle, a record of instantaneous sedimentation rates can be determined for each core. The core tops are given adjusted shipboard depth assignments (with the exception of Core 175-1085A-8H). The final age assignments are made by multiplying the approximate age by a correction factor. A second spectral analysis was performed using these $\delta^{18}O$ *C. wuellerstorfi* adjusted ages for verifying the fit in phase between cycles. Cores 175-1085A-9H and 10H ended up with overlapping cycles. This was corrected for by adding 35.72 k.y. to Core 175-1085A-10H ages. This had the effect of (1) diminishing the overlap, (2) keeping the tie points within the error bars, and (3) matching Cores 175-1085A-9H and 10H in such a fashion as to have the obliquity cycles at a matching phase for the end of one and the top of the other.

The label "final," of course, refers to the present study only. A more detailed reevaluation of magnetic properties and color sequences collected on board may make additional adjustments in age assignments advisable.

Figure F1. Location of Site 1085, off southern Namibia, showing the various oceanographic factors influencing the record: coastal upwelling (which is especially vigorous near Luederitz); Benguela Current (a mixture of waters from the South Atlantic Current, upwelled coastal waters, waters from the warm Agulhas Current, and occasional contributions from the Antarctic Circumpolar Current); and Agulhas Eddies spawned by the retroflection of the Agulhas Current moving south along the eastern shores of South Africa. Source: Berger and Wefer (1996), after Lutjeharms and van Ballegooyen (1988) as redrawn by Peterson and Stramma (1991).

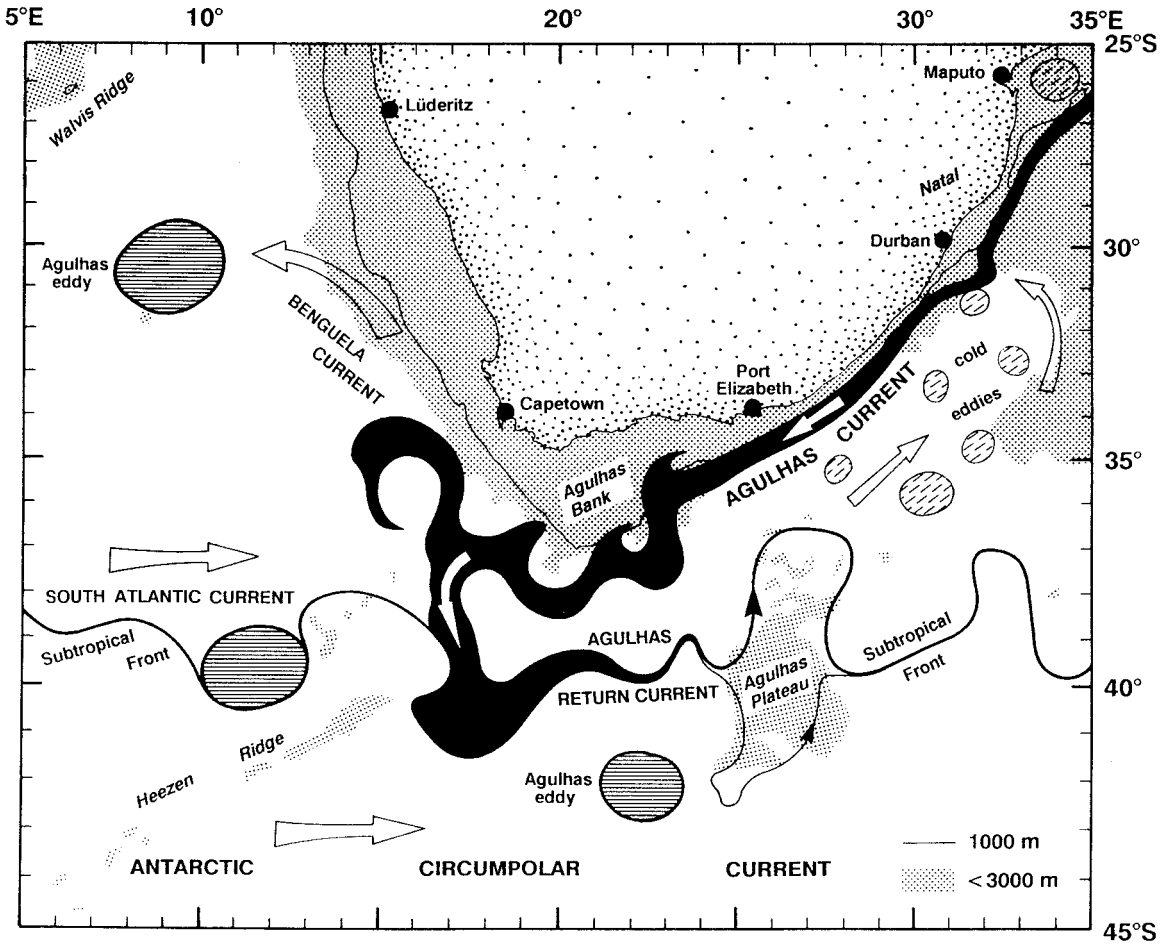

Figure F2. Sedimentation rates obtained from depth adjustments and age assignments as described in "Depth and Age Assignments," p. 5, and the "Appendix," p. 15, (see Table T1, p. 26). Stratigraphic tie points (Wefer et al., 1998; see explanations for the "Appendix," p. 15) are marked by a small square, with estimated error bars.

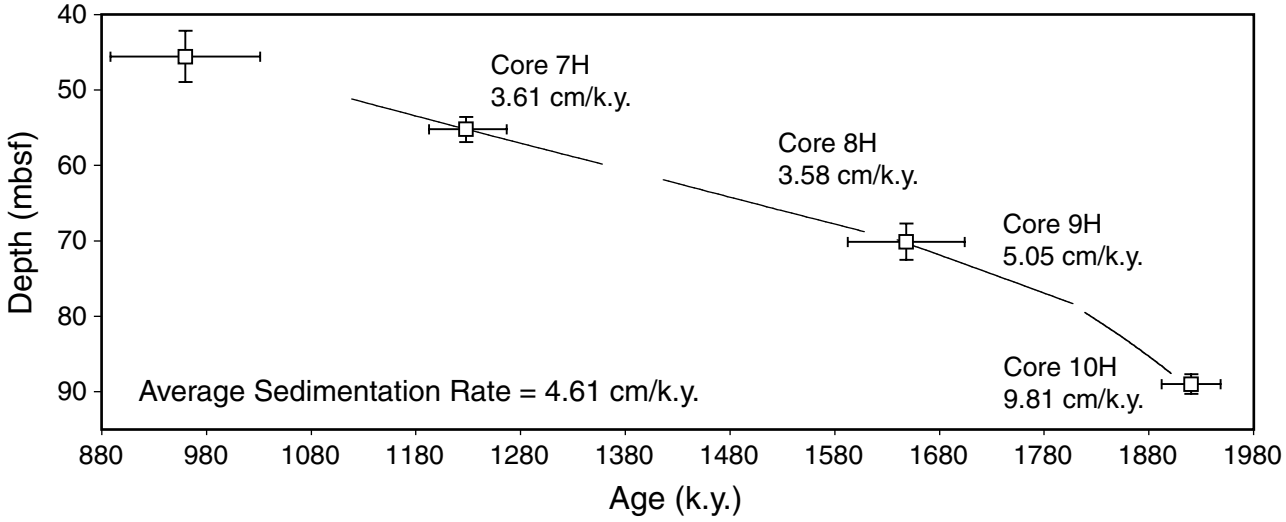

Figure F3. Stable isotope record of Cores 175-1085A-7H, 8H, 9H, and 10H.

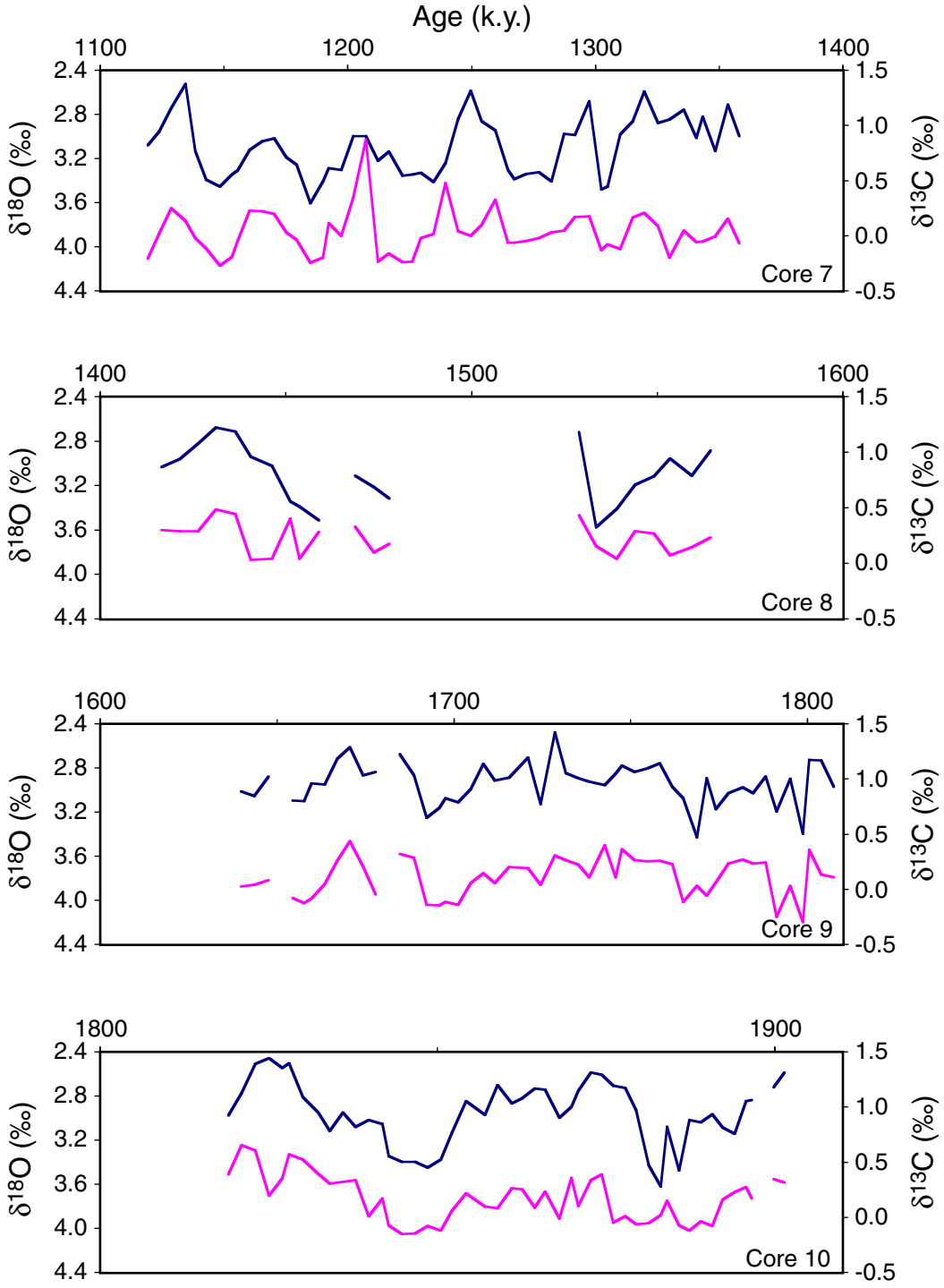

Figure F4. Correlation between oxygen isotope and carbon isotope series, as a function of lead and lag, in kiloyears. $\delta^{18}O$ is leading to the left of zero value. The two series seem well aligned, within a few thousand years.

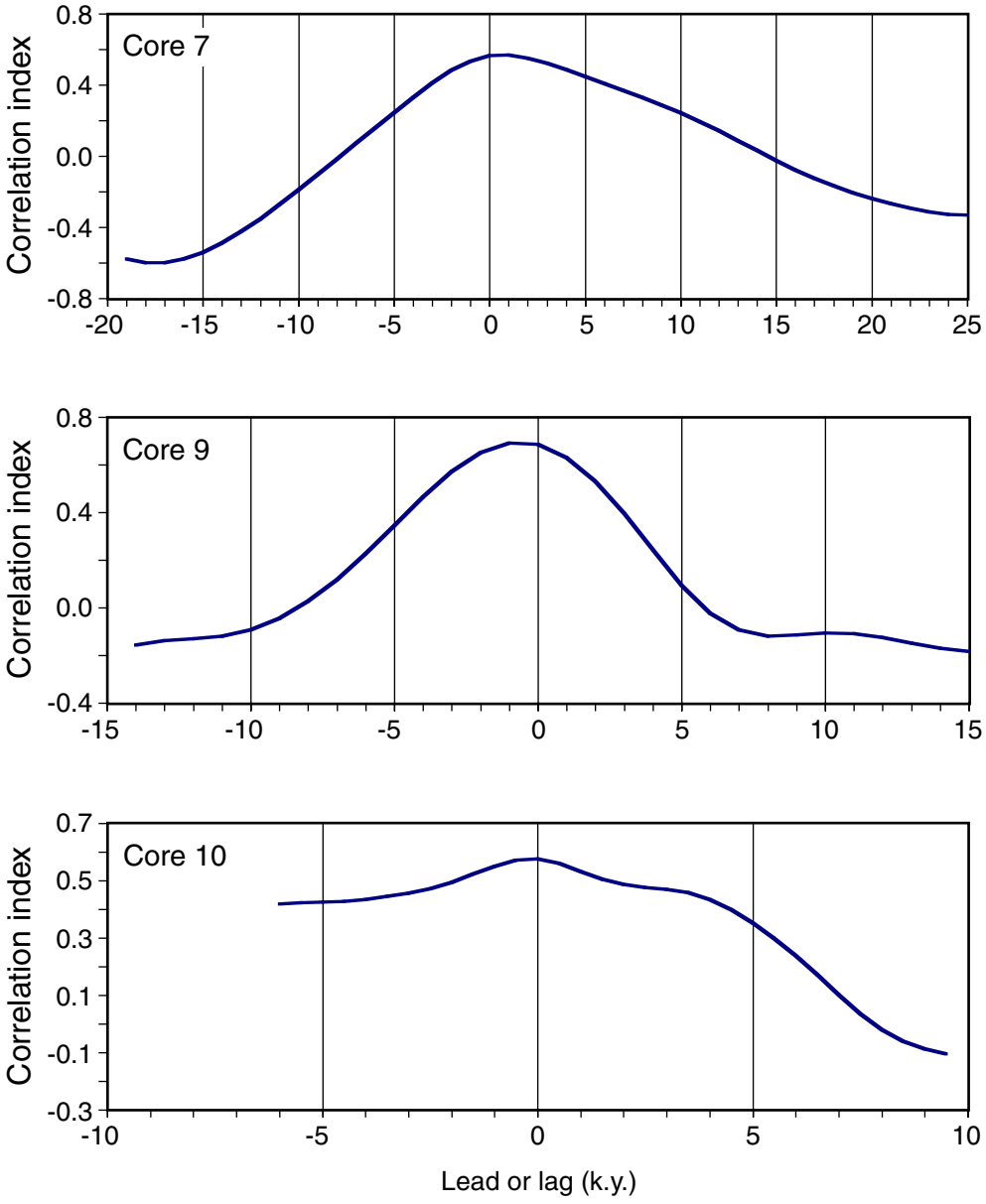

Figure F5. Fourier spectrum of the $\delta^{18}O$ stratigraphy of the cores studied, using the sedimentation rate based on tuning to the 41-k.y. cycle. **A.** Core 175-1085A-7H. Note the dominant peak at 41 k.y. and the cycles near 100 and 23 k.y. Also note the 67-k.y. cycle, resulting from the beating of the 100-k.y. cycle with the 41-k.y. cycle: $(100 \times 41)/(100-41)$. **B.** Core 175-1085A-8H. **C.** Core 175-1085A-9H. **D.** Core 175-1085A-10H.

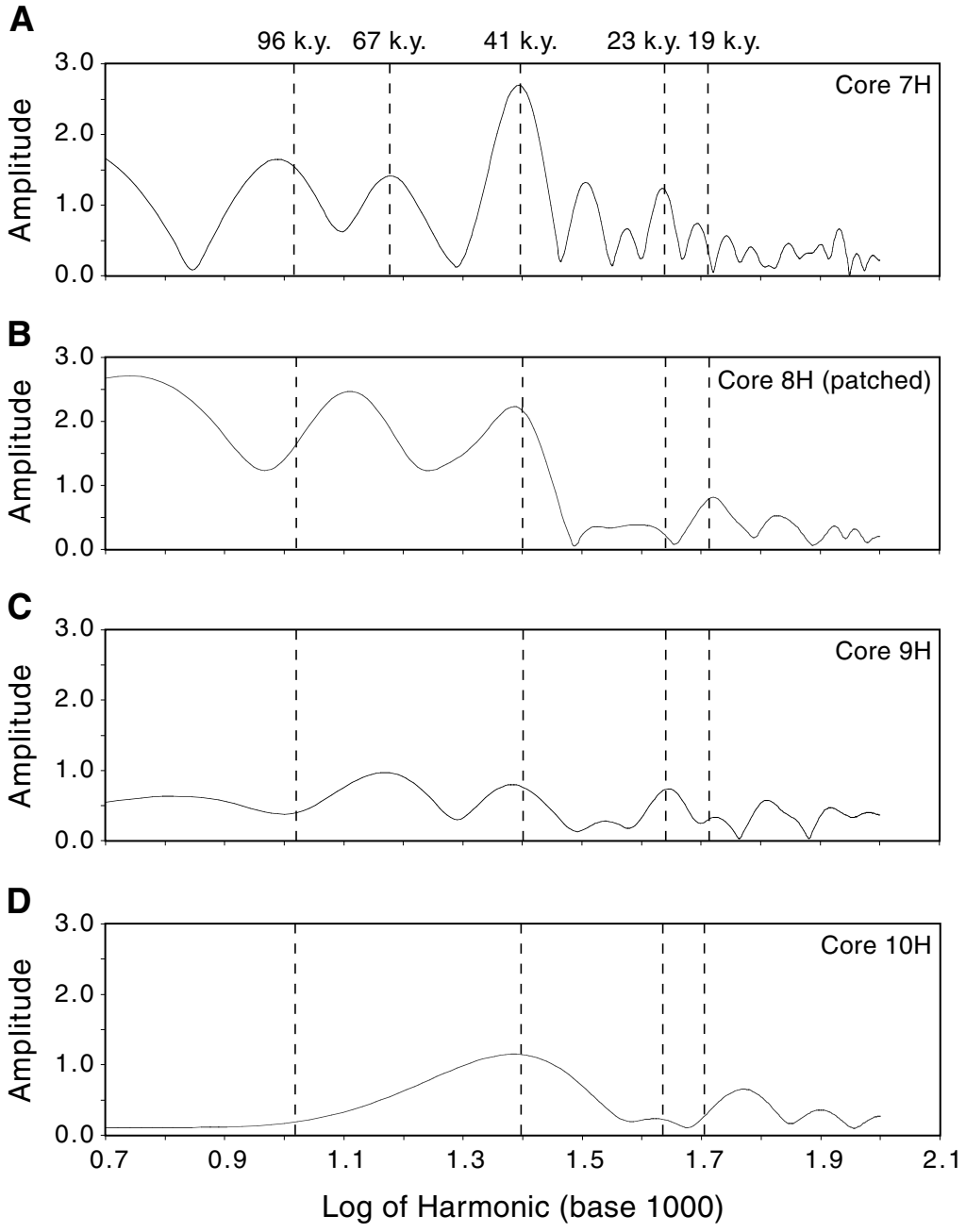

Figure F6. Benthic foraminifer abundance compared with climatic state as seen in oxygen isotopes of *C. wuellerstorfi*. **A.** Core 175-1085A-7H. **B.** Core 175-1085A-8H. **C.** Core 175-1085A-9H. **D.** Core 175-1085A-10H. The isotope record of Core 175-1085A-8H contains adjusted data from *Uvigerina peregrina*.

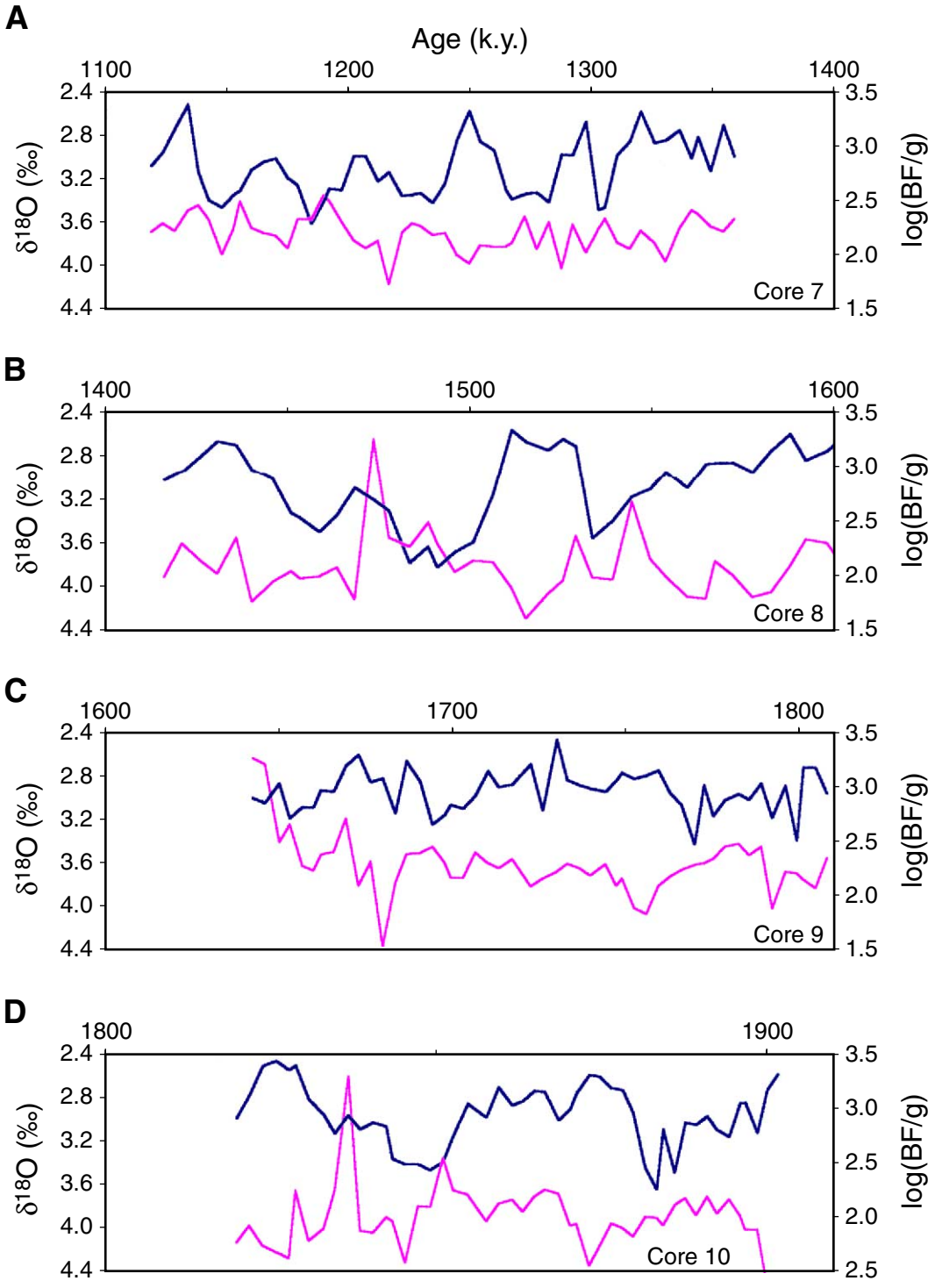

Figure F7. Comparison of $\delta^{18}O$ and EDA within the 41-k.y. cycle. The upper plot shows raw and filtered oxygen isotope data. Bandwidth is from 31 to 51 k.y. The lower plot shows filtered data for both $\delta^{18}O$ and EDA.

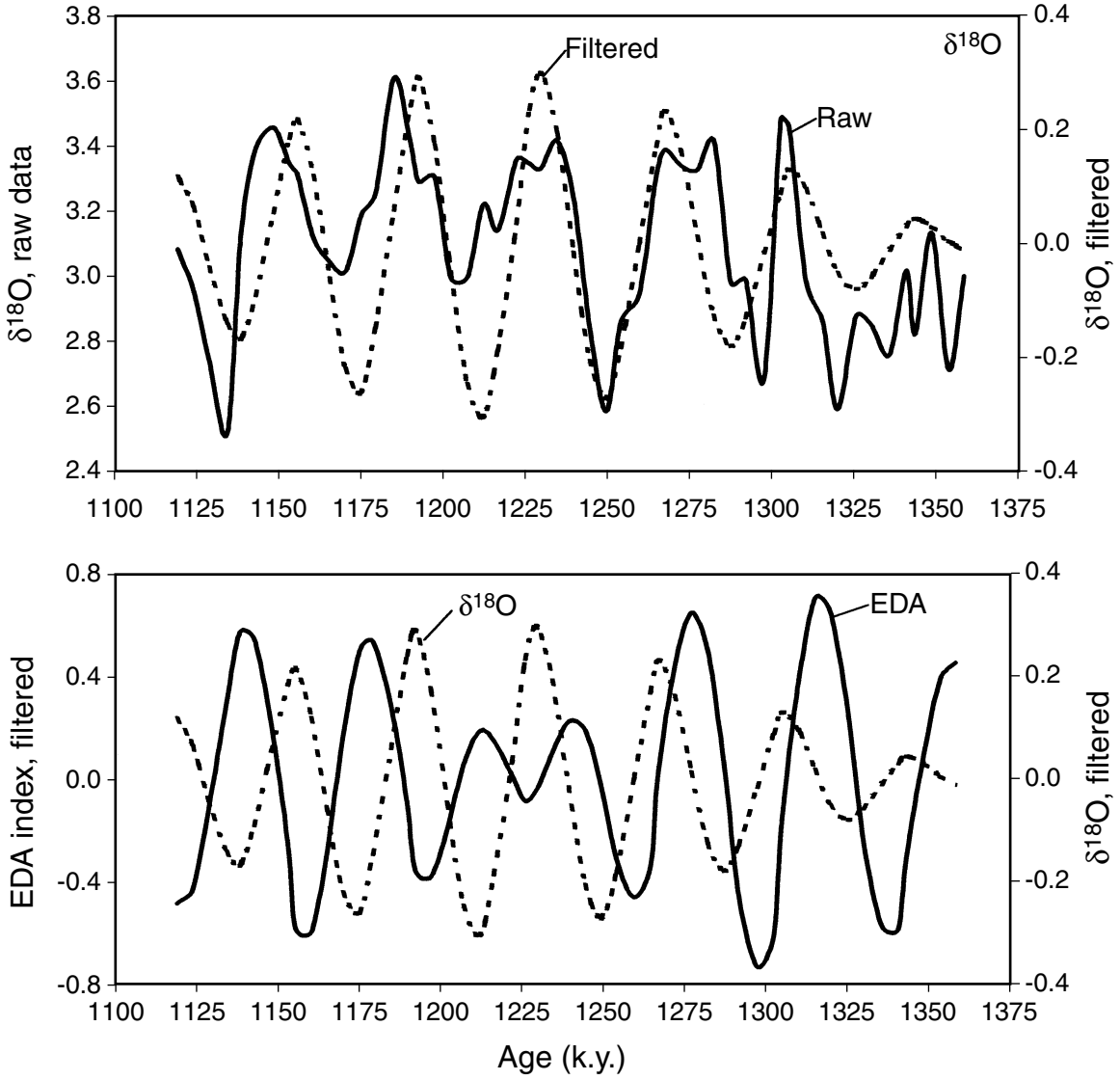

Figure F8. Modular plots for Core 175-1085A-7H, with comparison of variation in the proxies compared with the climate state as reflected by $\delta^{18}O$. All values are standardized. Csand = coarse sand.

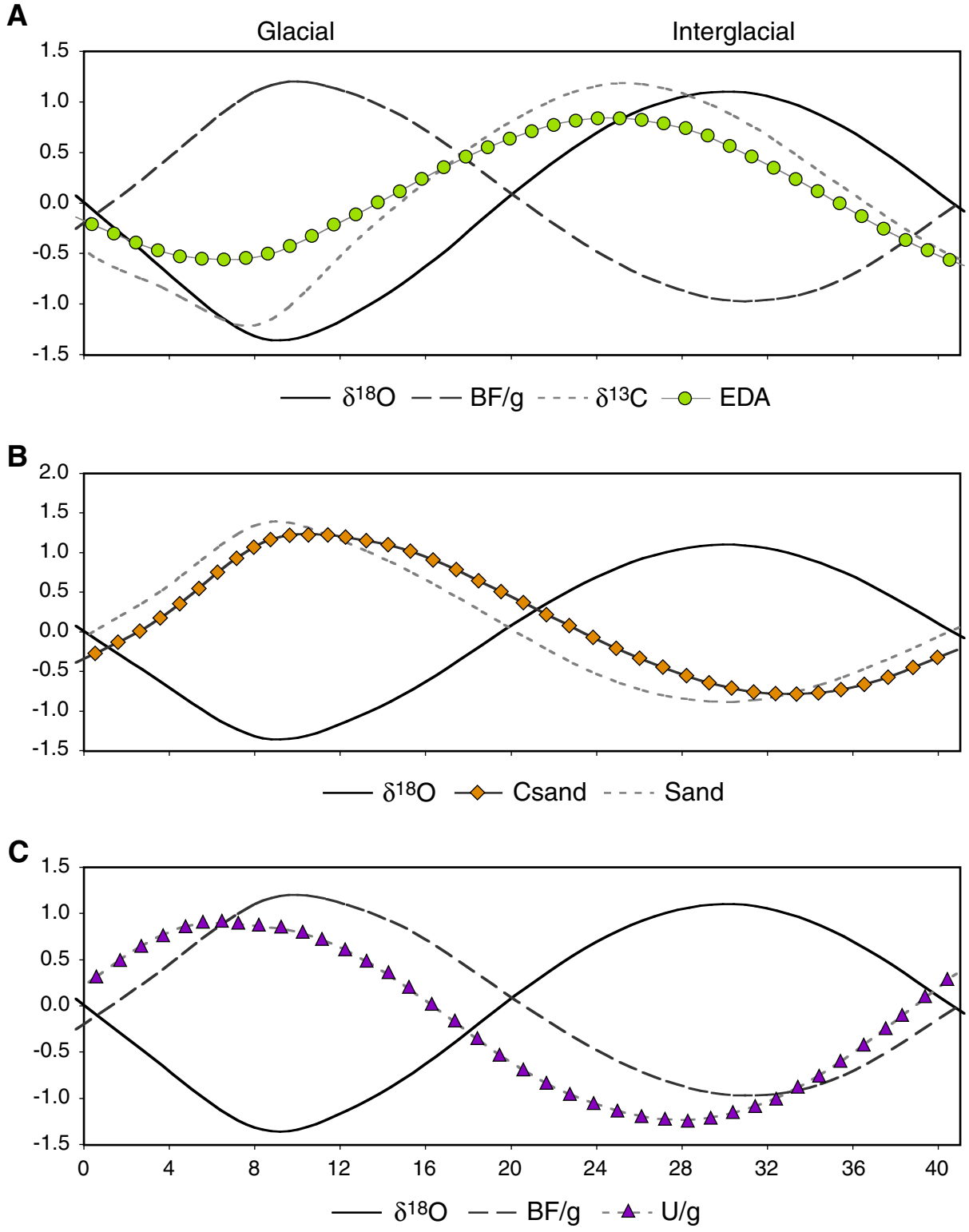

Figure F9. Relative strength of upwelling and mixing wind for Core 175-1085A-7H, from modular analysis. 41-k.y. cycles were extracted by Fourier filtering and then stacked.

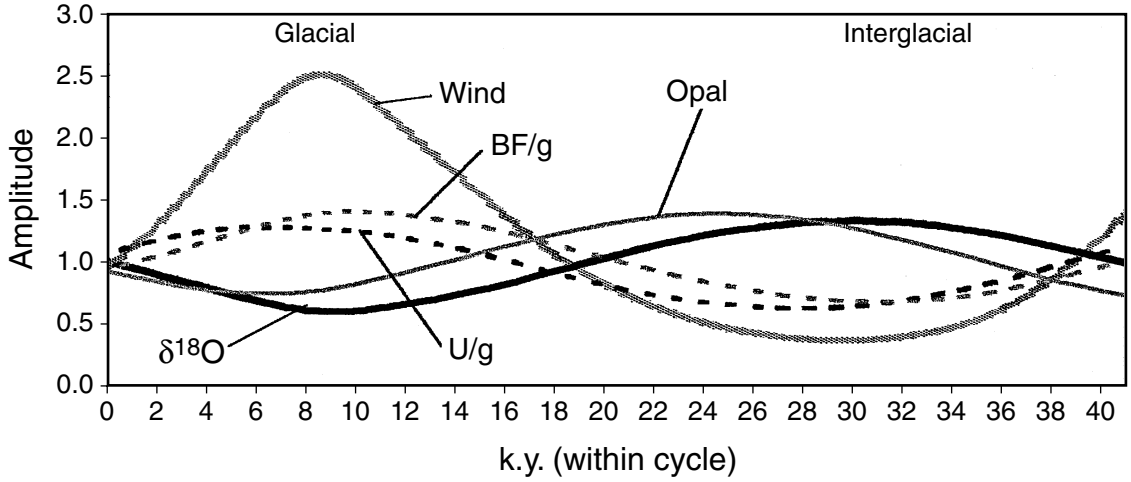

Table T1. Sedimentation rate adjustments based on Fourier analysis of oxygen isotope record.

Core	Shipboard sedimentation rate corrected for expansion (cm/k.y.)	41-k.y. cycle seen at (ka)	Correction factor (derived from Fourier analysis)	New sedimentation rate based on correction factor (cm/k.y.)
175-1085A-				
7H	3.51	42.11	1.03	3.61
8H	3.58	41.00	1.00	3.58
9H	6.42	32.26	0.79	5.05
10H	7.86	48.71	1.19	9.81*

Note: * = after two iterations.

Table AT1. Data for Hole 1085A. (**See table notes.** Continued on next four pages.)

Core, section, interval (cm)	Sample number	Upper depth (mbsf)	Revised depth (mbsf)	Final depth (mbsf)	Initial age by upper depth (ka)	Final age estimate (ka)	%Sand (total dry sediment)	% Coarse sand >250 µm (total sand)	*C. wuellerstorfi* $\delta^{18}O$ (‰)	*C. wuellerstorfi* $\delta^{13}C$ (‰)	*Uvigerina peregrina* $\delta^{18}O$ (‰)	*Uvigerina peregrina* $\delta^{13}C$ (‰)	$\delta^{18}O$ index (‰)	$\delta^{13}C$ index (‰)	*Uvigerina*/g	BF/g 150–250 µm	EDA smear slides	SOA	Comments
175-1085A-																			
7H-1, 2-4	99	51.22	51.22	51.22	1119	1119	14	6	3.08	–0.21	3.44	–0.62	3.08	–0.21	4.91	167	2	1	1, 7, 8
7H-1, 22-24	100	51.42	51.40	51.40	1125	1124	14	6	2.96	0.02	3.71	–1.01	2.96	0.02	5.55	200	3	1	1, 7
7H-1, 42-44	101	51.62	51.58	51.58	1131	1129	10	4	2.74	0.25	3.82	–1.05	2.74	0.25	3.60	171	4	2	1
7H-1, 62-64	102	51.85	51.79	51.79	1137	1134	9	4	2.52	0.14	—	—	2.52	0.14	2.40	263	5	2	1
7H-1, 82-84	103	52.02	51.94	51.94	1142	1138	16	11	3.13	–0.02	—	—	3.13	–0.02	8.43	290	3	1	1
7H-1, 100-102	104	52.20	52.10	52.10	1148	1143	18	4	3.39	–0.12	—	—	3.39	–0.12	11.46	217	2	1	1, 3, 7
7H-1, 122-124	105	52.42	52.30	52.30	1154	1148	11	11	3.46	–0.27	—	—	3.46	–0.27	7.97	105	2	0	1
7H-1, 142-144	106	52.62	52.48	52.48	1160	1153	16	6	3.35	–0.19	—	—	3.35	–0.19	4.37	179	2	0	1
7H-2, 2-4	107	52.72	52.57	52.57	1163	1156	24	8	3.31	–0.05	—	—	3.31	–0.05	2.88	317	2	0	1
7H-2, 22-24	108	52.92	52.75	52.75	1169	1160	10	7	3.12	0.23	—	—	3.12	0.23	2.62	182	2	0	1, 8
7H-2, 42-44	109	53.12	52.93	52.93	1175	1165	9	3	3.05	0.22	—	—	3.05	0.22	5.00	163	2	2	1, 8
7H-2, 62-64	110	53.32	53.11	53.11	1180	1170	10	6	3.02	0.20	3.74	–0.92	3.02	0.20	4.19	154	1	2	1, 6, 8
7H-2, 82-84	111	53.52	53.29	53.29	1186	1175	9	3	3.19	0.03	3.78	–0.98	3.19	0.03	2.85	119	1	1	1, 6, 8
7H-2, 99-101	112	53.69	53.44	53.44	1191	1179	10	5	3.26	–0.04	—	—	3.26	–0.04	6.00	218	2	1	1
7H-2, 122-124	113	53.92	53.65	53.65	1198	1185	15	9	3.61	–0.24	—	—	3.61	–0.24	13.90	220	2	0	1
7H-2, 142-144	114	54.12	53.83	53.83	1204	1190	18	5	3.41	–0.20	3.92	–1.34	3.41	–0.20	14.73	356	1	1	1, 6
7H-3, 2-4	115	54.22	53.92	53.92	1207	1192	14	8	3.29	0.11	3.96	–1.14	3.29	0.11	19.00	317	1	1	1, 6
7H-3, 22-24	116	54.42	54.10	54.10	1213	1197	10	7	3.30	0.00	3.75	–0.89	3.30	0.00	10.00	206	1	2	1, 2
7H-3, 42-44	117	54.62	54.28	54.28	1219	1202	8	4	3.00	0.35	—	—	3.00	0.35	4.42	140	2	2	1
7H-3, 62-64	118	54.82	54.46	54.46	1225	1207	9	4	3.00	0.87	—	—	3.00	0.87	3.20	118	2	2	1
7H-3, 82-84	119	55.02	54.64	54.64	1231	1212	9	3	3.22	–0.24	—	—	3.22	–0.24	3.69	138	2	2	1
7H-3, 100-102	120	55.20	54.80	54.80	1236	1217	8	6	3.14	–0.16	—	—	3.14	–0.16	2.23	56	2	2	1, 3, 8
7H-3, 122-124	121	55.42	55.00	55.00	1243	1222	15	9	3.36	–0.24	—	—	3.36	–0.24	8.29	166	2	1	1
7H-3, 138-140	122	55.58	55.14	55.14	1248	1226	10	9	3.35	–0.24	3.95	–1.43	3.35	–0.24	7.19	199	1	2	1, 6
7H-4, 2-4	123	55.72	55.27	55.27	1252	1230	9	11	3.33	–0.02	—	—	3.33	–0.02	5.14	187	1	1	1
7H-4, 22-24	124	55.92	55.45	55.45	1257	1235	8	14	3.41	0.02	—	—	3.41	0.02	5.83	156	2	1	1
7H-4, 42-44	125	56.12	55.63	55.63	1263	1240	7	8	3.24	0.48	—	—	3.24	0.48	7.38	163	3	2	1, 8
7H-4, 62-64	126	56.32	55.81	55.81	1268	1245	7	6	2.84	0.04	—	—	2.84	0.04	0.88	103	2	4	1, 5, 8
7H-4, 82-84	127	56.52	55.99	55.99	1273	1250	8	3	2.59	0.00	—	—	2.59	0.00	1.50	87	2	2	1, 3, 8
7H-4, 100-102	128	56.70	56.15	56.15	1278	1254	8	7	2.86	0.10	—	—	2.86	0.10	8.21	127	2	3	1, 5
7H-4, 122-124	129	56.92	56.35	56.35	1284	1260	5	4	2.95	0.33	—	—	2.95	0.33	6.42	122	3	3	1, 8
7H-4, 142-144	130	57.12	56.53	56.53	1289	1265	8	4	3.31	–0.07	—	—	3.31	–0.07	8.36	123	3	1	1, 8
7H-5, 2-4	131	57.22	56.62	56.62	1292	1267	8	7	3.39	–0.06	—	—	3.39	–0.06	16.64	132	2	1	1, 8
7H-5, 22-24	132	57.42	56.80	56.80	1297	1272	12	8	3.34	–0.05	—	—	3.34	–0.05	16.00	231	3	1	1, 8
7H-5, 42-44	133	57.62	56.98	56.98	1303	1277	6	9	3.32	–0.02	—	—	3.32	–0.02	1.80	116	3	2	1, 8
7H-5, 62-64	134	57.82	57.16	57.16	1308	1282	12	8	3.41	0.03	—	—	3.41	0.03	5.35	203	3	1	1
7H-5, 82-84	135	58.02	57.34	57.34	1314	1287	6	5	2.98	0.05	—	—	2.98	0.05	2.40	78	3	3	1
7H-5, 100-102	136	58.20	57.50	57.50	1319	1292	7	5	2.99	0.17	—	—	2.99	0.17	2.47	195	2	3	1
7H-5, 122-124	137	58.42	57.70	57.70	1325	1297	8	3	2.68	0.18	—	—	2.68	0.18	6.20	108	1	1	1, 8
7H-5, 142-144	138	58.62	57.88	57.88	1330	1302	8	5	3.48	–0.13	—	—	3.48	–0.13	22.60	177	2	1	1
7H-6, 2-4	139	58.72	57.97	57.97	1333	1305	9	6	3.46	–0.08	—	—	3.46	–0.08	24.13	220	2	1	1
7H-6, 22-24	140	58.92	58.15	58.15	1338	1310	8	5	2.98	–0.12	—	—	2.98	–0.12	16.60	134	2	3	1, 5
7H-6, 42-44	141	59.12	58.33	58.33	1344	1315	10	9	2.86	0.17	—	—	2.86	0.17	12.84	118	3	3	2, 4, 5
7H-6, 62-64	142	59.30	58.49	58.49	1348	1320	8	6	2.59	0.21	—	—	2.59	0.21	9.08	171	3	4	5
7H-6, 82-84	143	59.52	58.69	58.69	1354	1325	10	8	2.88	0.09	—	—	2.88	0.09	6.34	132	4	4	2, 4, 5

Table AT1 (continued).

Core, section, interval (cm)	Sample number	Upper depth (mbsf)	Revised depth (mbsf)	Final depth (mbsf)	Initial age by upper depth (ka)	Final age estimate (ka)	%Sand (total dry sediment)	% Coarse sand >250 µm (total sand)	*C. wuellerstorfi* $\delta^{18}O$ (‰)	*C. wuellerstorfi* $\delta^{13}C$ (‰)	*Uvigerina peregrina* $\delta^{18}O$ (‰)	*Uvigerina peregrina* $\delta^{13}C$ (‰)	$\delta^{18}O$ index (‰)	$\delta^{13}C$ index (‰)	*Uvigerina*/g	BF/g 150–250 µm	EDA smear slides	SOA	Comments
7H-6, 100-102	144	59.70	58.85	58.85	1359	1330	9	12	2.85	–0.20	—	—	2.85	–0.20	3.60	90	2	4	1, 5, 10
7H-6, 122-124	145	59.92	59.05	59.05	1365	1336	8	11	2.76	0.05	—	—	2.76	0.05	24.78	179	2	2	1, 7
7H-6, 142-144	146	60.12	59.23	59.23	1371	1341	8	11	3.02	–0.06	—	—	3.02	–0.06	19.88	262	2	1	1
7H-7, 2-4	147	60.22	59.32	59.32	1374	1343	9	11	2.82	–0.06	—	—	2.82	–0.06	22.33	240	1	1	1, 7
7H-7, 22-24	148	60.42	59.50	59.50	1379	1348	9	11	3.13	–0.01	—	—	3.13	–0.01	29.53	186	1	1	1
7H-7, 42-44	149	60.62	59.68	59.68	1385	1354	9	11	2.71	0.16	—	—	2.71	0.16	65.58	167	1	1	1
7H-7, 60-62	150	60.80	59.84	59.84	1389	1358	10	11	3.00	–0.07	—	—	3.00	–0.07	16.36	218	1	2	1, 7
8H-1, 2-4	151	60.72	60.72	61.94	1387	1417	5	11	3.04	0.30	—	—	3.04	0.30	9.93	93	4	2	2, 3, 4
8H-1, 22-24	152	60.92	60.90	62.12	1393	1421	8	12	2.96	0.29	3.92	–0.64	2.96	0.29	41.44	191	4	1	1, 3
8H-1, 42-44	153	61.12	61.08	62.30	1398	1426	5	9	2.82	0.29	3.93	–0.62	2.82	0.29	22.33	133	3	2	1
8H-1, 61-63	154	61.31	61.25	62.47	1403	1431	5	7	2.68	0.48	3.43	–0.61	2.68	0.48	23.04	101	4	3	1
8H-1, 82 84	155	61.52	61.44	62.66	1409	1436	7	12	2.72	0.44	3.54	–0.51	2.72	0.44	52.04	215	4	3	1
8H-1, 99-101	156	61.69	61.59	62.81	1414	1441	6	11	2.94	0.03	3.86	–0.61	2.94	0.03	4.06	56	1	2	1
8H-1, 122-124	157	61.92	61.80	63.02	1420	1446	7	10	3.03	0.04	4.04	–0.86	3.03	0.04	4.79	84	1	1	1
8H-1, 142-144	158	62.12	61.98	63.20	1426	1451	6	8	3.34	0.40	4.46	–0.91	3.34	0.40	3.16	106	2	1	1
8H-2, 2-4	159	62.22	62.07	63.29	1429	1454	5	8	3.39	0.04	4.38	–1.04	3.39	0.04	2.05	90	1	1	1
8H-2, 23-25	160	62.43	62.26	63.48	1434	1459	6	7	3.52	0.29	4.31	–0.46	3.52	0.29	6.23	95	1	1	1
8H-2, 42-44	161	62.62	62.43	63.65	1440	1464	8	10	—	—	4.28	–0.65	3.36	0.44	10.05	115	1	2	1
8H-2, 62-64	162	62.82	62.61	63.83	1445	1469	7	8	3.11	0.33	3.91	–0.80	3.11	0.33	15.46	58	2	3	1, 8
8H-2, 82-84	163	63.02	62.79	64.01	1451	1474	8	14	3.22	0.10	3.87	–0.78	3.22	0.10	15.39	1745	1	3	1
8H-2, 99-101	164	63.19	62.94	64.16	1456	1478	9	7	3.32	0.17	4.08	–0.86	3.32	0.17	78.85	216	1	2	1
8H-2, 122-124	165	63.42	63.15	64.37	1462	1484	9	13	—	—	4.72	–1.10	3.80	–0.01	12.78	178	2	1	1
8H-2, 142-144	166	63.62	63.33	64.55	1468	1489	12	10	3.65	0.19	4.84	–1.45	3.65	0.19	23.36	297	1	1	1
8H-3, 2-4	167	63.72	63.42	64.64	1470	1491	9	10	—	—	4.76	–1.09	3.84	–0.01	21.19	188	1	1	1
8H-3, 21-23	168	63.91	63.59	64.81	1476	1496	8	11	—	—	4.62	–1.00	3.70	0.09	3.27	105	1	2	1
8H-3, 41-43	169	64.11	63.77	64.99	1481	1501	7	5	—	—	4.53	–0.81	3.61	0.27	3.45	132	2	2	1
8H-3, 62-64	170	64.32	63.96	65.18	1487	1506	9	6	—	—	4.09	–0.97	3.17	0.12	3.28	128	1	3	1, 8
8H-3, 82-84	171	64.52	64.14	65.36	1493	1511	7	6	—	—	3.49	–1.29	2.57	–0.21	1.11	75	1	4	1, 3, 5, 8
8H-3, 98-100	172	64.68	64.28	65.50	1497	1515	6	4	—	—	3.60	–0.87	2.68	0.21	1.28	39	1	5	1
8H-3, 122-124	173	64.92	64.50	65.72	1504	1521	6	4	—	—	3.68	–1.04	2.76	0.05	1.22	66	2	3	1, 8
8H-3, 138-140	174	65.08	64.64	65.86	1508	1525	9	8	—	—	3.57	–0.90	2.65	0.19	6.57	88	2	3	1
8H-4, 2-4	175	65.22	64.77	65.99	1512	1529	9	7	2.72	0.44	3.80	–0.71	2.72	0.44	2.56	223	3	2	1
8H-4, 20-22	176	65.40	64.93	66.15	1517	1533	9	8	3.57	0.15	4.34	–1.03	3.57	0.15	6.90	93	3	2	1, 7, 8
8H-4, 42-44	177	65.62	65.13	66.35	1524	1539	8	13	3.41	0.04	4.33	–1.30	3.41	0.04	3.13	89	2	2	1, 8, 9
8H-4, 62-64	178	65.82	65.31	66.53	1529	1544	12	8	3.19	0.29	4.31	–1.09	3.19	0.29	1.38	457	2	1	1, 8, 9
8H-4, 82-84	179	66.02	65.49	66.71	1535	1549	8	9	3.12	0.27	4.06	–1.04	3.12	0.27	2.20	137	3	2	1, 8, 9
8H-4, 99-101	180	66.19	65.64	66.86	1540	1553	10	5	2.96	0.07	3.97	–0.96	2.96	0.07	1.04	96	2	2	1
8H-4, 122-124	181	66.42	65.85	67.07	1546	1559	7	5	3.11	0.14	3.78	–0.96	3.11	0.14	4.18	62	2	2	1, 3
8H-4, 142-144	182	66.62	66.03	67.25	1552	1564	6	5	2.89	0.23	3.73	–0.79	2.89	0.23	1.75	59	2	5	1, 5
8H-5, 2-4	183	66.72	66.12	67.34	1555	1567	6	8	—	—	3.80	–1.46	2.88	–0.37	2.27	131	2	5	1, 5
8H-5, 21-23	184	66.91	66.29	67.51	1560	1572	5	6	—	—	3.79	–1.26	2.87	–0.17	2.50	97	2	6	1, 5
8H-5, 42-44	185	67.12	66.48	67.70	1566	1577	5	5	—	—	3.88	–1.24	2.96	–0.15	4.67	62	2	6	1, 5
8H-5, 62-64	186	67.32	66.66	67.88	1572	1582	6	3	—	—	3.68	–0.95	2.76	0.14	1.45	68	1	7	1, 5, 8
8H-5, 82-84	187	67.52	66.84	68.06	1577	1587	7	4	—	—	3.53	–0.74	2.61	0.34	3.55	119	2	6	1, 5, 8
8H-5, 99-101	188	67.69	66.99	68.21	1582	1592	8	7	—	—	3.77	–0.72	2.85	0.37	5.24	208	1	6	1, 5
8H-5, 122-124	189	67.92	67.20	68.42	1589	1598	9	5	—	—	3.68	–0.88	2.76	0.20	7.50	191	2	5	1, 5
8H-5,142-144	190	68.12	67.38	68.60	1595	1603	6	3	—	—	3.53	–0.93	2.62	0.15	3.74	108	2	6	1, 3, 5

Table AT1 (continued).

Core, section, interval (cm)	Sample number	Upper depth (mbsf)	Revised depth (mbsf)	Final depth (mbsf)	Initial age by upper depth (ka)	Final age estimate (ka)	%Sand (total dry sediment)	% Coarse sand >250 µm (total sand)	*C. wuellerstorfi* $\delta^{18}O$ (‰)	*C. wuellerstorfi* $\delta^{13}C$ (‰)	*Uvigerina peregrina* $\delta^{18}O$ (‰)	*Uvigerina peregrina* $\delta^{13}C$ (‰)	$\delta^{18}O$ index (‰)	$\delta^{13}C$ index (‰)	*Uvigerina*/g	BF/g 150–250 µm	EDA smear slides	SOA	Comments
8H-CC, 2-4	191	68.18	67.43	68.65	1596	1604	6	5	—	—	3.43	–0.71	2.51	0.37	18.12	142	1	7	2, 3, 4, 5
8H-CC, 18-20	192	68.34	67.58	68.80	1601	1608	10	8	—	—	3.65	–0.83	2.73	0.26	11.40	125	2	3	1, 2, 3, 4
9H-1, 5-8	1	70.25	70.25	69.90	1656	1640	9	10	3.01	0.03	—	—	3.01	0.03	31.50	1796	1	1	1
9H-1, 25-28	2	70.45	70.43	70.08	1662	1643	9	6	3.06	0.04	—	—	3.06	0.04	14.60	1571	2	1	1
9H-1, 48-51	3	70.68	70.64	70.29	1669	1648	5	10	2.88	0.08	—	—	2.88	0.08	12.60	306	1	1	1
9H-1, 65-68	4	70.85	70.79	70.44	1672	1651	4	4	—	—	—	—	3.20	0.07	14.00	441	1	3	1, 10
9H-1, 85-88	5	71.05	70.97	70.62	1675	1654	8	31	3.09	–0.08	—	—	3.09	–0.08	12.60	188	1	1	1, 3, 10
9H-1, 103-106	6	71.23	71.13	70.78	1678	1658	4	6	3.10	–0.13	—	—	3.10	–0.13	12.60	170	1	3	1, 5, 10
9H-1, 115-118	7	71.35	71.24	70.89	1680	1660	6	5	2.94	–0.09	—	—	2.94	–0.09	26.30	237	2	3	1, 3, 10
9H-1, 135-138	8	71.55	71.42	71.07	1683	1663	6	4	2.95	0.05	—	—	2.95	0.05	10.00	250	2	3	1, 3, 8, 10
9H-2, 5-8	9	71.75	71.60	71.25	1686	1667	6	4	2.72	0.26	—	—	2.72	0.26	17.60	506	1	3	1, 3, 5, 10
9H-2, 25-28	10	71.95	71.78	71.43	1689	1671	5	5	2.61	0.44	—	—	2.61	0.44	11.00	123	1	3	1, 3, 5, 10
9H-2, 48-51	11	72.15	71.96	71.61	1692	1674	5	6	2.87	0.21	—	—	2.87	0.21	15.60	205	1	3	1, 3, 5, 10
9H-2, 65-68	12	72.35	72.14	71.79	1695	1678	6	4	2.83	–0.05	—	—	2.83	–0.05	12.00	35	1	3	1, 5, 8, 10
9H-2, 85-88	13	72.55	72.32	71.97	1699	1681	11	5	—	—	—	—	3.15	–0.04	14.00	132	2	1	1, 3
9H-2, 103-106	14	72.73	72.48	72.13	1701	1685	10	5	2.68	0.32	—	—	2.68	0.32	19.30	241	2	1	1
9H-2, 125-128	15	72.95	72.68	72.33	1705	1689	8	9	2.87	0.29	—	—	2.87	0.29	18.20	244	1	1	1
9H-2, 145-148	16	73.15	72.86	72.51	1708	1692	10	11	3.25	–0.14	—	—	3.25	–0.14	75.50	281	2	1	1
9H-3, 5-8	17	73.35	73.04	72.69	1711	1696	6	6	3.17	–0.15	—	—	3.17	–0.15	26.00	200	2	1	1
9H-3, 25-28	18	73.45	73.13	72.78	1713	1698	6	5	3.07	–0.12	—	—	3.07	–0.12	70.70	145	2	1	1, 3
9H-3, 45-48	19	73.65	73.31	72.96	1716	1701	6	4	3.11	–0.14	—	—	3.11	–0.14	16.30	146	2	2	1, 3, 10
9H-3, 65-68	20	73.85	73.49	73.14	1719	1705	8	7	2.99	0.06	—	—	2.99	0.06	26.40	247	2	2	1, 3, 10
9H-3, 85-88	21	74.05	73.67	73.32	1722	1708	8	6	2.76	0.14	3.33	–0.10	2.76	0.14	11.70	199	1	4	1, 6, 10
9H-3, 103-106	22	74.23	73.83	73.48	1725	1712	9	7	2.91	0.06	3.57	–1.05	2.91	0.06	12.10	179	1	4	1, 6, 10
9H-3, 125-128	23	74.45	74.03	73.68	1728	1716	8	9	2.89	0.20	—	—	2.89	0.20	15.70	216	3	3	2, 3, 6, 10
9H-4, 5-8	24	74.75	74.30	73.95	1732	1721	6	8	2.71	0.19	3.22	–1.02	2.71	0.19	12.20	122	3	4	1, 10
9H-4, 25-28	25	74.95	74.48	74.13	1735	1724	6	6	3.13	0.04	—	—	3.13	0.04	10.60	143	2	4	1, 10
9H-4, 48-51	26	75.18	74.69	74.34	1739	1729	5	6	2.48	0.31	3.95	–1.30	2.48	0.31	15.00	166	3	3	1, 6, 10
9H-4, 65-68	27	75.35	74.84	74.49	1741	1732	14	12	2.85	0.26	—	—	2.85	0.26	10.80	196	4	1	2, 3, 4
9H-4, 85-88	28	75.55	75.02	74.67	1744	1735	10	9	2.90	0.22	—	—	2.90	0.22	12.00	178	4	1	2, 3, 4
9H-4, 103-106	29	75.73	75.18	74.83	1747	1738	9	5	2.92	0.11	—	—	2.92	0.11	10.80	153	2	3	2, 3, 10
9H-4, 127-130	30	75.97	75.40	75.05	1751	1743	11	6	2.96	0.40	—	—	2.96	0.40	22.30	193	3	2	2, 7, 10
9H-4, 145-148	31	76.15	75.56	75.21	1753	1746	8	6	2.85	0.11	—	—	2.85	0.11	21.50	123	3	2	1, 5, 10
9H-5, 5-8	32	76.25	75.65	75.30	1755	1748	7	9	2.78	0.36	—	—	2.78	0.36	28.00	143	2	3	1, 3, 10
9H-5, 25-28	33	76.45	75.83	75.48	1758	1751	9	12	2.84	0.27	—	—	2.84	0.27	18.10	77	2	1	2, 3, 4
9H-5, 45-48	34	76.65	76.01	75.66	1761	1755	10	8	2.81	0.25	—	—	2.81	0.25	17.30	68	2	2	2, 3, 4
9H-5, 65-68	35	76.85	76.19	75.84	1764	1758	15	8	2.76	0.26	—	—	2.76	0.26	16.50	123	2	2	2, 3, 4
9H-5, 85-88	36	77.05	76.37	76.02	1767	1762	14	9	2.97	0.23	—	—	2.97	0.23	9.80	150	2	2	2, 3, 4
9H-5, 103-106	37	77.23	76.53	76.18	1769	1765	10	6	3.07	–0.11	—	—	3.07	–0.11	12.30	172	3	2	2, 3, 4, 7
9H-5, 125-128	38	77.45	76.73	76.38	1773	1769	7	10	3.43	0.03	—	—	3.43	0.03	16.50	190	1	1	2, 3, 4
9H-5, 145-148	39	77.60	76.87	76.52	1775	1771	10	8	2.90	–0.06	3.96	–1.30	2.90	–0.06	16.20	199	3	1	2, 3, 4, 6
9H-6, 5-8	40	77.75	77.00	76.65	1777	1774	11	10	3.18	0.06	4.03	–1.21	3.18	0.06	17.20	219	2	1	2, 3, 4, 6
9H-6, 25-28	41	77.95	77.18	76.83	1780	1778	9	8	3.03	0.23	3.73	–1.34	3.03	0.23	14.20	280	2	1	2, 3, 4, 6, 7
9H-6, 48-51	42	78.18	77.39	77.04	1783	1782	15	12	2.98	0.27	3.75	–1.27	2.98	0.27	13.10	295	3	1	2, 3, 4, 6
9H-6, 65-68	43	78.35	77.54	77.19	1786	1785	15	12	3.03	0.24	3.68	–0.96	3.03	0.24	11.50	233	3	1	2, 3, 4, 6
9H-6, 85-88	44	78.55	77.72	77.37	1788	1788	21	8	2.88	0.24	3.48	–1.04	2.88	0.24	12.10	279	2	1	2, 3, 4, 6
9H-6, 103-106	45	78.73	77.88	77.53	1791	1791	9	5	3.19	–0.25	—	—	3.19	–0.25	19.30	77	2	2	2, 3, 4, 6

Table AT1 (continued).

Core, section, interval (cm)	Sample number	Upper depth (mbsf)	Revised depth (mbsf)	Final depth (mbsf)	Initial age by upper depth (ka)	Final age estimate (ka)	%Sand (total dry sediment)	% Coarse sand >250 µm (total sand)	*C. wuellerstorfi* $\delta^{18}O$ (‰)	*C. wuellerstorfi* $\delta^{13}C$ (‰)	*Uvigerina peregrina* $\delta^{18}O$ (‰)	*Uvigerina peregrina* $\delta^{13}C$ (‰)	$\delta^{18}O$ index (‰)	$\delta^{13}C$ index (‰)	*Uvigerina*/g	BF/g 150–250 µm	EDA smear slides	SOA	Comments
9H-6, 125-158	46	78.95	78.08	77.73	1794	1795	11	5	2.90	0.03	—	—	2.90	0.03	15.40	166	2	1	2, 3, 4, 10
9H-6, 145-148	47	79.15	78.26	77.91	1797	1799	9	6	3.40	–0.30	—	—	3.40	–0.30	19.40	160	2	1	2, 3, 4, 10
9H-7, 5-8	48	79.25	78.35	78.00	1798	1800	11	8	2.73	0.36	—	—	2.73	0.36	17.00	141	2	2	2, 3, 4, 10
9H-7, 25-28	49	79.45	78.53	78.18	1801	1804	17	7	2.73	0.13	—	—	2.73	0.13	14.00	118	2	1	2, 3, 4
9H-7, 45-48	50	79.65	78.71	78.36	1804	1807	7	5	2.97	0.11	—	—	2.97	0.11	16.00	221	1	3	1
10H-1, 65-68	51	80.36	80.36	79.52	1814	1819	5	3	2.98	0.39	3.24	–1.03	2.98	0.39	3.50	62	1	4	1, 5, 6
10H-1, 5-88	52	80.55	80.53	79.69	1817	1821	5	4	2.77	0.65	—	—	2.77	0.65	4.40	88	1	3	1, 3, 10
10H-1, 105-108	53	80.75	80.71	79.87	1819	1823	4	6	2.51	0.61	3.31	–0.93	2.51	0.61	7.00	59	4	3	1, 3, 6, 7, 10, 11
10H-1, 125-128	54	80.95	80.89	80.05	1822	1825	4	5	2.46	0.20	—	—	2.46	0.20	10.40	50	3	3	1, 6, 10
10H-1, 145-148	55	81.15	81.07	80.23	1825	1827	6	6	2.54	0.35	3.09	–0.90	2.54	0.35	10.70	45	2	3	1, 3, 6
10H-2, 5-8	56	81.25	81.16	80.32	1826	1828	5	5	2.50	0.57	3.27	–0.83	2.50	0.57	9.70	183	2	3	1, 6, 9
10H-2, 25-28	57	81.45	81.34	80.50	1829	1830	5	6	2.81	0.53	—	—	2.81	0.53	10.90	64	2	3	1, 10
10H-2, 48-51	58	81.68	81.55	80.71	1832	1832	5	3	2.95	0.39	3.49	–0.07	2.95	0.39	3.60	83	1	4	1, 3, 7, 10
10H-2, 65-68	59	81.85	81.70	80.86	1835	1834	5	4	3.12	0.31	—	—	3.12	0.31	5.88	185	1	3	1, 3, 10
10H-2, 85-88	60	82.05	81.88	81.04	1837	1836	5	6	2.95	0.32	—	—	2.95	0.32	10.96	1990	2	3	1, 3, 10
10H-2, 104-107	61	82.24	82.05	81.21	1840	1838	6	5	3.08	0.34	—	—	3.08	0.34	8.53	80	2	2	1, 3, 7, 10
10H-2, 124-127	62	82.44	82.23	81.39	1843	1840	7	4	3.02	0.01	3.57	–1.11	3.02	0.01	6.10	75	1	1	1, 3, 6
10H-2, 145-148	63	82.65	82.42	81.58	1845	1842	9	5	3.06	0.17	4.14	–1.10	3.06	0.17	4.35	105	2	1	2, 4, 6
10H-3, 5-8	64	82.75	82.51	81.67	1847	1843	18	8	3.35	–0.07	3.84	–0.08	3.35	–0.07	2.42	97	1	1	2, 4, 6
10H-3, 25-28	65	82.95	82.69	81.85	1849	1845	6	4	3.40	–0.15	4.16	–1.07	3.40	–0.15	2.44	41	2	2	2, 4, 6
10H-3, 45-48	66	83.15	82.87	82.03	1852	1847	8	6	3.40	–0.15	4.14	–1.16	3.40	–0.15	3.35	132	2	1	1, 6
10H-3, 65-68	67	83.35	83.05	82.21	1855	1849	8	4	3.45	–0.08	3.87	–1.06	3.45	–0.08	2.54	130	2	2	1, 6, 7, 8
10H-3, 85-88	68	83.55	83.23	82.39	1857	1850	15	7	3.38	–0.12	—	—	3.38	–0.12	3.22	361	2	2	1, 3
10H-3, 102-105	69	83.72	83.38	82.54	1860	1852	13	8	3.14	0.06	—	—	3.14	0.06	3.55	184	3	1	1
10H-3, 125-128	70	83.95	83.59	82.75	1863	1854	11	5	2.85	0.22	—	—	2.85	0.22	6.58	168	3	2	1, 3
10H-4, 5-8	71	84.25	83.86	83.02	1867	1857	6	6	2.97	0.10	—	—	2.97	0.10	4.48	97	3	2	1
10H-4, 25-28	72	84.45	84.04	83.20	1869	1859	12	7	2.70	0.08	—	—	2.70	0.08	6.01	140	5	2	2, 4, 11
10H-4, 48-51	73	84.68	84.25	83.41	1872	1861	7	6	2.87	0.27	—	—	2.87	0.27	10.31	152	4	2	1, 2
10H-4, 65-68	74	84.85	84.40	83.56	1874	1863	7	6	2.82	0.25	—	—	2.82	0.25	11.66	119	4	3	1, 2
10H-4, 85-88	75	85.05	84.58	83.74	1877	1864	14	11	2.73	0.09	—	—	2.73	0.09	3.79	162	4	2	2, 3, 7, 11
10H-4, 102-105	76	85.22	84.73	83.89	1879	1866	11	7	2.75	0.23	—	—	2.75	0.23	6.47	188	3	2	2, 3
10H-4, 125-158	77	85.45	84.94	84.10	1882	1868	7	6	3.00	–0.01	—	—	3.00	–0.01	4.09	173	4	2	2, 3
10H-4, 145-148	78	85.65	85.12	84.28	1885	1870	11	7	2.90	0.36	—	—	2.90	0.36	3.39	88	5	2	2, 4, 10
10H-5, 6-9	79	85.76	85.22	84.38	1886	1871	8	6	2.75	0.10	—	—	2.75	0.10	2.45	91	5	3	2, 4, 10, 11
10H-5, 27-30	80	85.97	85.41	84.57	1889	1873	10	13	2.59	0.34	—	—	2.59	0.34	3.13	38	5	2	2, 4, 10, 11
10H-5, 45-48	81	86.15	85.57	84.73	1891	1874	7	2	2.61	0.39	—	—	2.61	0.39	4.20	57	4	2	1, 3, 10
10H-5, 65-68	82	86.35	85.75	84.91	1894	1876	7	4	2.71	–0.05	—	—	2.71	–0.05	4.07	93	5	2	1, 3, 10
10H-5, 85-88	83	86.55	85.93	85.09	1896	1878	8	6	2.73	0.01	—	—	2.73	0.01	2.90	84	5	2	1
10H-5, 103-106	84	86.73	86.09	85.25	1898	1879	7	5	2.93	–0.07	—	—	2.93	–0.07	5.76	71	5	2	1, 3
10H-5, 125-128	85	86.95	86.29	85.45	1901	1881	8	7	3.43	–0.05	—	—	3.43	–0.05	2.68	106	5	2	2, 3, 10
10H-5, 145-148	86	87.15	86.47	85.63	1904	1883	19	13	3.62	0.02	—	—	3.62	0.02	2.64	103	3	2	2, 3, 10, 11
10H-6, 6-9	87	87.26	86.57	85.73	1905	1884	7	6	3.08	0.15	—	—	3.08	0.15	2.60	89	3	2	1, 3, 10
10H-6, 27-30	88	87.47	86.76	85.92	1908	1886	11	9	3.47	–0.08	—	—	3.47	–0.08	9.20	136	4	2	1, 10
10H-6, 45-48	89	87.65	86.92	86.08	1910	1887	15	9	3.02	–0.12	—	—	3.02	–0.12	21.66	158	4	2	1, 10
10H-6, 65-68	90	87.85	87.10	86.26	1912	1889	8	5	3.04	–0.04	—	—	3.04	–0.04	7.32	110	5	2	1, 10
10H-6, 85-88	91	88.05	87.28	86.44	1915	1891	9	9	2.97	–0.08	3.53	–0.75	2.97	–0.08	13.42	163	6	2	1
10H-6, 103-106	92	88.23	87.44	86.60	1917	1892	7	9	3.09	0.16	3.51	–0.78	3.09	0.16	8.56	115	6	2	1

Table AT1 (continued).

Core, section, interval (cm)	Sample number	Upper depth (mbsf)	Revised depth (mbsf)	Final depth (mbsf)	Initial age by upper depth (ka)	Final age estimate (ka)	%Sand (total dry sediment)	% Coarse sand >250 µm (total sand)	*C. wuellerstorfi* $\delta^{18}O$ (‰)	*C. wuellerstorfi* $\delta^{13}C$ (‰)	*Uvigerina peregrina* $\delta^{18}O$ (‰)	*Uvigerina peregrina* $\delta^{13}C$ (‰)	$\delta^{18}O$ index (‰)	$\delta^{13}C$ index (‰)	*Uvigerina*/g	BF/g 150–250 µm	EDA smear slides	SOA	Comments
10H-6, 125-128	93	88.45	87.64	86.80	1920	1894	7	7	3.15	0.23	3.92	–1.45	3.15	0.23	6.50	152	6	1	1, 6
10H-6, 145-148	94	88.65	87.82	86.98	1922	1896	8	7	2.85	0.28	3.64	–1.14	2.85	0.28	8.05	109	6	1	1, 6, 8
10H-7, 5-8	95	88.75	87.91	87.07	1923	1897	7	6	2.84	0.17	3.55	–1.07	2.84	0.17	6.10	81	6	1	1, 6, 8
10H-7, 27-30	96	88.97	88.11	87.27	1926	1898	6	8	—	—	3.43	–1.02	3.11	0.09	3.97	81	6	3	1, 6, 8, 10
10H-7, 45-48	97	89.15	88.27	87.43	1928	1900	8	15	2.72	0.35	3.60	–0.97	2.72	0.35	2.24	25	6	3	1, 6, 7, 10
10H-7, 65-68	98	89.35	88.45	87.61	1931	1901	8	7	2.59	0.32	3.64	–0.96	2.59	0.32	6.95	16	6	3	1, 6, 8, 10

Notes: Hole 1085A is located at 29°22.5′S, 13°59.4′E in 1713.2 m water depth. Penetration in Hole 1085A was 604 mbsf. — = no data available. EDA = estimated diatom abundance, SOA = sulfide and oxide aggregates. Comments: 1 = clean sample; 2 = clumps; 3 = fibers; 4 = cement; 5 = casts; 6 = *Uvigerina* matrix; 7 = fish teeth, bones, and otoliths; 8 = radiolarians; 9 = sponge spicules; 10 = orange metal;, 11 rounded corners from too much sieve.